Arctic spring and summertime aerosol optical depth baseline from long-term observations and model reanalyses~~, with implications for the impact of regional biomass burning processes~~ - Part 1: climatology and trend

Peng Xian[1], Jianglong Zhang[2], Travis D. Toth[3], Blake Sorenson[2], Peter R. Colarco[4], Zak Kipling[5], Norm T. O'Neill[6], Edward J. Hyer[1], James R. Campbell[1], Jeffrey S. Reid[1] and Keyvan Ranjbar[6]

[1]Naval Research Laboratory, Monterey, CA, USA.
[2]Department of Atmospheric Sciences, University of North Dakota, Grand Forks, ND
[3]NASA Langley Research Center, Hampton, Virginia, USA.
[4]NASA Goddard Space Flight Center, Greenbelt, MD, USA.
[5]European Centre for Medium-Range Weather Forecasts, Reading, UK.
[6]Département de géomatique appliqué, Université de Sherbrooke, Sherbrooke, Québec, Canada

Correspondence: Peng Xian (peng.xian@nrlmry.navy.mil)

Style Definition: Comment Text

Abstract

We present an Arctic aerosol optical depth (AOD) climatology and trend analysis for 2003-2019 spring and summertime periods derived from a combination of multi-agency aerosol reanalyses, remote sensing retrievals, and ground observations. This includes the U.S. Navy Aerosol Analysis and Prediction System ReAnalysis version 1 (NAAPS-RA v1), the NASA Modern-Era Retrospective Analysis for Research and Applications, version 2 (MERRA-2), and the Copernicus Atmosphere Monitoring Service ReAnalysis (CAMSRA). Space-borne remote sensing retrievals of AOD are considered from the Moderate Resolution Imaging Spectroradiometer (MODIS), the Multi-angle Imaging SpectroRadiometer (MISR), and Cloud-Aerosol Lidar with Orthogonal Polarization (CALIOP). Ground-based data include sun photometer data from Aerosol Robotic Network (AERONET) sites and oceanic Maritime Aerosol Network (MAN) measurements. Aerosol reanalysis AODs and space-borne retrievals show consistent climatological spatial patterns and trends for both spring and summer seasons over the lower-Arctic (60-70°N). Consistent ~~signs in the~~ AOD ~~trend~~trends are also found for the high Arctic (north of 70°N) from reanalyses. The aerosol reanalyses yield more consistent AOD results than climate models, verify well with AERONET, and corroborate complementary climatological and trend analysis. Speciated AODs are more variable than total AOD among the three reanalyses, and a little more so for March-May (MAM) than for June-August (JJA). Black Carbon (BC) AOD in the Arctic comes predominantly from biomass burning (BB) sources in both MAM and JJA, and ~~biomass burning~~BB overwhelms anthropogenic sources in JJA for the study period.

AOD exhibits a multi-year negative ~~trend in the Arctic in~~ MAM trend, and a positive ~~trend in~~ JJA trend in the Arctic during 2003-2019, due to an overall decrease in sulfate/anthropogenic ~~pollutions~~pollution, and a significant JJA increase in ~~biomass burning~~BB smoke ~~in JJA~~. Interannual Arctic AOD variability is significantly large, driven by fine-mode, and specifically, ~~biomass burning (BB)~~BB smoke, ~~though more so~~with both smoke contribution and interannual variation larger in JJA than in MAM. ~~Extreme AOD events during spring and summer in the~~ It is recommended that climate models should account for BB emissions and BB interannual variabilities and trends in Arctic~~, defined as AOD greater than the 95th percentile value, are mainly attributed to BB smoke transport events. Extreme AOD cases tend to occur later in the season (i.e., July and August, in the latter decade rather than spreading over April-August in the early decade during 2003-2019) corresponding to a shift to a later time in extreme boreal BB activities.~~

climate change studies.

Formatted: Space After: 10 pt

1. Introduction

The Arctic is warming faster than the overall global climate, a phenomenon widely known as Arctic amplification (Serreze and Francis 2006; Serreze and Barry 2011). This has led to rapid changes in regional sea ice properties. September sea ice coverage is shrinking at an unprecedented rate (Comiso 2012; Meier et al., 2014). Younger and thinner ice is replacing thick multi-year sea ice (Kwok and Rothrock 2009; Hansen et al, 2013; Rosel et al. 2018). Mechanisms contributing to sea ice changes include increased anthropogenic greenhouse gases (Notz and Stroeve 2016; Dai et al., 2019), sea ice-albedo feedback (Perovich and Polashenski 2012), increased warm and moist air intrusion into the Arctic (Boisvert et al. 2016; Woods et al., 2016; Graham et al. 2017), radiative feedbacks associated with cloudiness and humidity (Kapsch et al. 2013; Morrison et al. 2018), and increased ocean heat transport (Nummelin et al., 2017; Taylor et al. 2018). However, one of the least understood factors of Arctic change is the impact of aerosols on sea ice albedo and concentration (IPCC 2013).

Atmospheric aerosol particles from anthropogenic and natural sources reach the Arctic region through both long-range transport and local emissions, affecting regional energy balance through both direct and indirect radiative processes (Quinn et al., 2008; Engvall et al., 2009; Flanner, 2013; Sand et al., 2013; Markowicz et al., ~~2018~~2021; Yang et al., 2018). Aerosol particles influence cloud microphysical properties as cloud condensation nuclei (CCN) and/or ice nuclei (IN), affecting cloud albedo, lifetime, phase, and probability of precipitation (e.g~~.~~., Lubin and Vogelmann, 2006; Lance et al., 2011; Zamora et al, 2016; Zhao and Garrett 2015; Bossioli et al., 2021). Additionally, deposition of light-absorbing aerosol species such as dust and black/brown carbon on the surface of snow and ice can trigger albedo feedbacks and facilitate melting and prolong melting seasons (Hansen & Nazarenko, 2004; Jacobson, 2004; Flanner et al., 2007; Skiles et al., 2018; Dang et al., 2017; Kang et al., 2020). However, the impact of aerosol particles on polar climate change is still not well characterized, and their relative importance compared to other warming factors is difficult to isolate and quantify.

Climate modeling studies show that due to stronger feedback processes between the atmosphere-ocean-sea-ice-land the Arctic region is more sensitive to local changes in radiative forcing than tropical and mid-latitude regions (Shindell and Faluvegi 2009; Sand et al., 2013). On the other hand, there seems to be an emerging agreement on a higher sensitivity of Arctic clouds by aerosol particles than lower-latitude regions due to the very low aerosol amounts compared to lower latitudes (Prenni et al., 2007; Mauritsen et al. 2011; Birch et al., 2012; Coopman et al., 2018; Wex et al., 2019). Both ~~suggest~~underscore the important role aerosol particles may play in the Arctic weather and climate, and the urgency to better quantify the amount of aerosols in the Arctic.

A variety of atmospheric aerosol species exist in the Arctic region. Anthropogenic pollution contributes significantly to the formation of the Arctic haze, which ~~often~~generally occurs in later winter and spring due to wintertime build-up in the shallow boundary layer with effective transport and reduced removal (e.g., Law and Stohl, 2007; Quinn et al., 2008). Biomass burning (BB) smoke, originating from wildfires in boreal North America and Eurasia, are often observed and/or modeled being transported into the Arctic (Eck et al. 2009; Eckhardt et al. 2015; Stohl et al. 2007; Warneke et al. 2009; Iziomon et al., 2006; Evangeliou et al. 2016; Kondo et al., 2011; Brieder et al., 2014; Markowicz et al. 2016; Khan et al., 2017; Engelmann et al., 2021). Airborne dust, emitted from exposed sand or soils due to glacier retreat (Bullard et al., 2016; Groot Zwaaftink et al., 2016), are likely on the rise as the Arctic warms. Dust can also originate from lower latitude deserts, e.g~~.~~., Sahara and Asia, and arrive in the Arctic through long-range transport (Stone et al, 2007; Breider et al., 2014~~).~~; AboEl-Fetouh et al., 2020). As the Arctic sea-ice melts and ~~opens up~~ the ~~ocean~~ice-free surface increases, emissions of sea salt and biogenic aerosols (e.g., from dimethylsulfide; Dall et al., 2017; Gabric et al., 2018) are expected to increase. There are also ultrafine particles nucleated from gaseous precursors, though in small amounts (Baccarini et al., 2021; Abbatt et al., 2019).

Because of the harsh surface environment endemic to the Arctic, aerosol field measurements are limited ~~compared~~in comparison with the mid-latitude and tropical environments. Despite an increasing number of field campaigns carried out ~~in~~over the past two decades (e.g~~.~~., review by Wendisch et al., 2019; and more recently the MOSAiC, https://mosaic-expedition.org) and their usefulness in improving process-level understanding, field measurement periods tend to be short and limited to certain areas and thus are not necessarily representative spatially and temporally of the whole Arctic. There are many ~~studies on~~ Arctic-aerosol optical ~~properties~~ property studies that are based on long-term site measurements (e.g~~.~~., Herber et al., 2002; Tomasi et al., 2007; Eck et al., 2009; ~~Saha et al., 2010;~~ Glantz et al., 2014; Ranjbar et al., 2019; AboEl-Fetouh et al., 2020), however, the number of ~~the~~ sites is limited~~,~~ and ~~the sites are~~ of irregular spacing (mostly located ~~on~~at the northern edge of the North American, Eurasian continents, and the Svalbard region~~, not yielding a continuous spatial distribution.~~).

Climate models ~~without constraint from~~that are not well constrained by observations exhibit large variations in basic aerosol optical properties, with an order of magnitude difference in simulated regional aerosol optical depth (AOD) and large differences in the simulated seasonal cycle of AOD over the Arctic (e.g~~.~~., Glantz et al., 2014; Sand et al., 2017). These results ~~do~~will not reduce the uncertainty in the radiative impact of aerosols through direct (including surface albedo effect) and indirect forcings in the Arctic climate. Impacts of aerosols and clouds, overall, constitute one of the largest sources of

uncertainty in climate models (IPCC 2013). This is apparently exacerbated in a warming Arctic (Goosse et al., 2018). A modeling study by DeRepentigny et al. (2021) shows that the inclusion of interannually varying BB emissions, compared with ~~using~~only climatological ~~ones alone, introduces a~~emissions, results in simulations of large Arctic climate variability and ~~enhances~~enhanced sea ice loss. This finding suggests the sensitivity of climate relevant processes to aerosol interannual variability in the Arctic.

In this paper, we present an AOD climatology~~,~~ and trend analysis ~~and extreme events statistics~~ for the 2003-2019 Arctic spring and summertime, based on a combination of multi-national interagency aerosol reanalyses, satellite remote sensing retrievals, and ground observations. We define the Arctic~~/~~ and the high-Arctic as regions north of 60°N~~/~~ and 70°N~~, and sub~~ respectively. The lower-Arctic is defined as regions between 60°N-70°N. To reference lower-latitude source influences, the area of 50°N-90°N is included for context.

There are clear advantages ~~of~~to using aerosol reanalyses ~~from~~of chemical transport models in comparison with climate models for Arctic aerosol studies. Smoke emissions are frequently updated (~~e.g., h~~ourly rather than monthly BB smoke emission~~) and~~ sources for example) while satellite observations of both meteorological and aerosol data are also incorporated into those aerosol reanalyses through data assimilation. High-latitude fires are strongly influenced by weather patterns including large-scale transport patterns (e.g~~.~~., Flannigan and Harrington 1998; Skinner et al. 1999). Thus, BB smoke in particular, is more realistically accounted for in aerosol reanalyses.

To our knowledge, this is the first time aerosol reanalysis products are evaluated and compared over the Arctic. The goal of the study is to provide a baseline of AOD distribution, magnitude, speciation, and interannual variability over the Arctic during the sea ice melting season~~, which~~. Statistics of Arctic extreme AOD events is provided in a companion paper (Part 2). The baseline can be used for evaluating aerosol models ~~and further~~, calculating aerosol radiative forcing, and providing background information for field campaign data analysis and future field campaign planning in a larger climate context. ~~The~~This paper is organized as follows: Sect. 2 and 3 introduce the data sets and methods respectively. Sect. 4 verifies the reanalyses. Results are reported in Sect. 5. Discussions and conclusions are provided in Sect. 6 and 7.

2. Data

A combination of aerosol reanalyses, satellite-based aerosol remote sensing ~~aerosol~~ data, and ground-based aerosol measurements are used to describe source dependent AOD and its trend over the Arctic during spring (March-May, ie., MAM) and summertime (June-August, ie., JJA). Note that “MAM” and “JJA” are meant to represent convenient and informative acronyms for springtime and summertime. In the sections where we

Formatted: Comment Text, Line spacing: Multiple 1.15 li

discuss MAM and JJA trends we refer to, respectively, year to year trends of springtime and summertime AODs (not seasonal trends from March to April to May or June to July to August averaged over the multi-year sampling period). The aerosol reanalyses include the Navy Aerosol Analysis and Prediction System reanalysis (NAAPS-RA; Lynch et al., 2016) developed at the Naval Research Laboratory, the NASA Modern-Era Retrospective Analysis for Research and Applications, version 2 (MERRA-2; Randles et al., 2017), and the Copernicus Atmosphere Monitoring Service ReAnalysis (CAMSRA; Inness et al., 2019) produced at ECMWF. The remote sensing data include AOD retrievals ~~of AOD~~ from the Moderate Resolution Imaging Spectroradiometer (MODIS; Levy et al., 2013), the Multi-angle Imaging SpectroRadiometer (MISR; Kahn et al., 2010), and Cloud-Aerosol Lidar with Orthogonal Polarization (CALIOP). Sun photometer data from ~~the~~ Aerosol Robotic Network (AERONET; Holben et al., 1998) sites and oceanic Maritime Aerosol Network (MAN, Smirnov et al., 2009) measurements ~~are also used.~~ Overviews of remote sensing techniques for Arctic aerosols can be found in Tomasi et al. (2015) and Kokhanovsky et al. (2020). The analysis period is focused on 2003-2019, when all three aerosol reanalyses are available. ~~Also, both Terra and Aqua Moderate Resolution Imaging Spectroradiometer (MODIS) AOD retrievals were ingested into those aerosol reanalyses through data assimilation. It is notable that MODIS AOD retrievals are very limited over the Arctic region due to snow and ice coverage as well as challenges in cloud-clearing over cold and bright surfaces. Still, we expect the assimilation of MODIS AOD over lower latitudes to provide certain constraints in AOD for those aerosol reanalyses over the Arctic region.~~ A summary of the datasets is provided in Appendix A.

2.1 MODIS AOD

AOD data from MODIS on Terra and Aqua was based on Collection 6.1 Dark Target and Deep Blue retrievals (Levy et al., 2013). Additional quality control and some corrections were applied as described in Zhang and Reid 2006, Hyer et al. 2011, Shi et al. 2011, and Shi et al. 2013, and were updated for the Collection 6.1 inputs. The quality-assured and quality-controlled MODIS C6 AOD data (550 nm) are a level 3 product that is produced at 1°x1° latitude/longitude spatial and 6-hrly temporal resolution. Those 6-hrly (averaged) MODIS AOD data were then monthly-binned in order to study long-term aerosol climatology and trends. Seasonal means and trends were derived only when the total count of 1°x1° degree and 6-hrly data was greater than 10 for a season.

2.2 MISR AOD

~~Onboard~~The MISR instrument onboard the Terra satellite platform~~, the MISR instrument~~ provides observations at nine different viewing zenith angles ~~at~~across four different

spectral bands ranging from 446 to 866 nm~~, allowing for~~. These instrumental configurations facilitate AOD retrievals over bright surfaces, such as desert regions (Kahn et al., 2010). MISR Version 23 AOD data at 558 nm (Garay et al., 2020) were analyzed between Jan 2003 and December 2019. No MISR AOD is available over Greenland due to snow and ice coverage. Monthly gridded MISR AOD data were created by averaging only MISR data with 100% clear pixels, as defined by each pixel's 'cloud screening parameter', at a spatial resolution of 1°x1° latitude/longitude. Only monthly grid cells whose number of MODIS 100%-cloud-clear AODs was greater than 20 were used to derive the climatology and trend.

2.3 CALIOP AOD

~~CALIOP,~~Cloud-Aerosol Lidar with Orthogonal Polarization (CALIOP), the primary instrument on the Cloud-Aerosol Lidar and Infrared Pathfinder Satellite Observations (CALIPSO) satellite, is a polarization-sensitive lidar that operates at two wavelengths (532 and 1064 nm; Winker et al. 2003). ~~Since~~It has, since its launch in 2006, ~~it has~~ collected a continuity of vertical ~~observations of atmospheric aerosols~~aerosol and ~~clouds for over fifteen years. The CALIPSO analyses for this study~~cloud profiles. We primarily ~~utilize~~utilized daytime and nighttime 532 nm aerosol extinction coefficient data from the Version 4.2 (V4.2) Level 2 (L2) aerosol profile product (5 km horizontal/60 m vertical resolution) (Kim et al., 2018), with the V4.2 L2 aerosol layer product used for quality assurance (QA) procedures. ~~-~~The CALIOP aerosol profiles are ~~rigorously QAed before analysis~~, as implemented and described in detail in past studies, rigorously QAed before analysis (Campbell et al. 2012; Toth et al. 2016; 2018).~~-~~ Only cloud-free CALIOP profiles are used, as determined through the atmospheric volume description (AVD) parameter included in the aerosol profile product (i.e., we ~~implement~~implemented a strict cloud screening procedure for which we ~~exclude~~excluded CALIOP profiles with any range bin classified as cloud by the AVD parameter). ~~Additionally, we note that a~~A significant portion of CALIOP aerosol profile data consists of retrieval fill values (-9999s, or RFVs~~), due~~) that are, in part, due to the minimum detection limits of the lidar.~~-~~ In fact, for some areas in the Arctic region, over 80% of CALIOP profiles consist entirely of RFVs (Toth et al. 2018). ~~-~~These result in column AODs being equal to zero~~, and as such~~; including them in the composites would artificially lower the mean AOD. ~~Thus, they are~~They were thus excluded from our analysis. We also tested retaining AOD=0 values in our analysis and that did not change the AOD trends (see more discussions in section 6). Lastly, the cloud-free QAed profiles without AOD ~~equal to zero~~=0 profiles ~~are~~were used to compute mean CALIOP ~~AOD~~AODs at 2° x 5° latitude/longitude resolution. To ensure spatial and temporal representation, seasonal means and trends ~~are~~were derived only when the total count of gridded data is ~~greater than 20 for a~~any season exceeded 20.

Formatted: Font color: Black

2.4 AERONET

The AErosol RObotic NETwork (AERONET) is a ground-based global ~~scale~~ sun photometer network. AERONET instruments measure sun and sky radiance at several wavelengths, ranging from the near-ultraviolet to the near-infrared. This network has been providing ~~high-accuracy~~ daytime measurements of aerosol properties since the 1990s (Holben et al., 1998; Holben et al., 2001). Only cloud-screened, quality-assured version 3 Level 2 AERONET data (Giles et al., 2019) are used in this study.

The 500 nm fine mode (FM) and coarse model (CM) AODs from the Spectral Deconvolution Method (SDA) of O'Neill et al. (2003), along with the FM spectral derivative at 500 nm are used to extrapolate FM AOD to 550 nm. It is assumed the CM AOD at 500 nm and 550 nm are equal. Total AOD ~~at 550 nm~~ is simply the sum of FM and CM AODs ~~at 550 nm~~. The SDA product is an AERONET product that has been verified using in situ measurements (see for example Kaku et al., 2014) and a variety of co-located lidar experiments (see, for example, Saha et al., 2010 and Baibakov et al., 2015). The FM and CM separation is effected spectrally: this amounts to a separation of the FM and CM optical properties associated with their complete FM and CM particle size distributions. This optical separation, characterized by the ratio of FM AOD to total AOD at 550 nm is referred to as the fine mode fraction (FMF). An analogous FM and CM AOD separation in terms of a cutoff radius applied to ~~the~~a retrieved or measured particle size distribution is referred to as the sub-micron fraction (SMF; where the numerator of the SMF is the FM AOD associated with the AOD contribution of particles below ~~the~~a cutoff radius). The SMF is the basis ~~of the comprehensive~~for separating FM and CM components in the AERONET (AOD & sky radiance) inversion. The SDA algorithm and the AERONET inversion generate FM and CM AODs that are moderately different (see Sect. 4 Kleidman et al., 2005~~): the~~). The advantage of the SDA is its significantly higher retrieval resolution (~ a few minutes versus ~ an hour for the AERONET inversion) and thus retrieval numbers, its independence from a variable cut off radius and its greater operational generality (being applicable to other networks such as the MAN sunphotometer network).

AERONET data ~~are~~were binned into 6-hr intervals centered at normal synoptic output times of the reanalyses (0, 6, 12, and 18 UTC) and then averaged within the bins. ~~Monthly~~ The monthly-mean ~~AERONET AOD is derived only when the count of 6-hr AERONET data exceeds 18 to ensure~~ temporal representativeness~~.~~ was rendered more likely by only including means with more than 18 6-hr data bins. Ten AERONET sites ~~were selected~~ (Table 1, Fig. 1) were selected based on regional representativeness (coupled with the reality of the sparsity of AERONET sites in the Arctic), the availability of data records between Jan 2003 and Dec 2019 (the main study period), and for easier comparison with other Arctic studies (e.g~~. Sand et al., 2017).~~., Sand et al., 2017). To

explore the potential impact of different sampling resolutions on the results (e.g., Balmes et al., 2021), we generated daily AOD statistics (Table S1) that could be compared with Table 1 6hrly statistics. In general, the mean and median of MAM or JJA AODs (including total, FM and CM AODs) at the ten AERONET sites change very slightly (mostly 0.00, or <=0.01). The daily AOD standard deviation was less than its 6hrly analogue.

We found that thin clouds could occasionally be identified and retrieved as CM aerosols in level 2, version 3 AERONET data. These retrievals were manually removed by identifying such thin clouds using Terra and Aqua visible-wavelength imagery from NASA Worldview and comparing 6-hrly NAAPS-RA with AERONET AODs. CM ~~AOD~~AODs greater than 3-sigma level ~~was~~were then also removed (as per AboEl-Fetouh et al., 2020).

2.5 MAN AOD

The Marine Aerosol Network (MAN) is a hand-held Microtops sun photometer (research vessel) counterpart to AERONET~~, available~~ employed for ~~over~~ ocean measurements in areas where ~~a standard Cimel sun photometer is not feasible~~no-land based AERONET site can exist (Smirnov et al., 2009, 2011). ~~-~~The products share AERONET nomenclature~~,~~ and data processing is similar to that of AERONET. ~~For this study, Level2~~Level 2 data above ~~60~~70°N for the period of 2003-2019 ~~are used.~~were employed in this study. SDA-based FM and CM AOD at 550 nm ~~are~~were derived ~~based on SDA (O'Neill et al., 2003)~~ and averaged over 6-hr time bins.

2.6 NAAPS AOD reanalysis v1

The Navy Aerosol Analysis and Prediction System (NAAPS) AOD ~~reanalysis~~ReAnalysis (NAAPS-RA) v1 provides 550 nm speciated AOD at a global scale with 1°x1° degree spatial and 6-hrly temporal resolution for the years 2003-2019 (Lynch et al., 2016). This reanalysis is based on NAAPS with assimilation of quality-controlled retrievals of AOD from MODIS and MISR (Zhang et al., 2006; Hyer et al., 2011; Shi et al., 2011). AODs from anthropogenic and biogenic fine aerosol species (ABF, a mixture of sulfate, BC, organic aerosols and secondary organic aerosols from non-BB sources), dust, biomass-burning smoke, and sea salt aerosols are available. The aerosol source functions were tuned to obtain the best match between the model FM and CM AODs and the AERONET AODs for 16 regions globally. Wet deposition processes were constrained with satellite-derived precipitation (Xian et al., 2009). The reanalysis reproduces the decadal AOD trends found using standalone satellite products ~~over the globe (except the polar regions due to lack of verification data) in other studies (e.g., Zhang et al., 2010; 2017). Note that although a first-of-its-kind Ozone Monitoring Instrument (OMI) data assimilation method has been developed for directly assimilation OMI Aerosol~~

~~Index (AI) over bright surfaces such as snow and ice covered regions (Zhang et al., 2021), research progress is on-going for developing data-assimilation quality OMI AI data over the Arctic region and thus, the OMI AI data assimilation is not included in this study.~~(e.g., Zhang et al., 2010; 2017 who excluded polar regions due to lack of verification data).

2.7 MERRA-2 AOD reanalysis

NASA Modern-Era Retrospective Analysis for Research and Applications, version 2 (MERRA-2) includes aerosol reanalysis, which incorporates assimilation of AOD from a variety of remote sensing sources, including MODIS and MISR after 2000. The aerosol module used for MERRA-2 is the Goddard Chemistry, Aerosol Radiation and Transport model (GOCART; Chin et al. 2000; Colarco et al., 2010), which provides simulations of sulfate, black and organic carbon, dust and sea salt aerosols. A detailed description and global validation of the AOD reanalysis product can be found in Randles et al. (2017) and Buchard et al. (2017). For this study, monthly mean speciated AODs and total AOD at 550 nm with 0.5° latitude and 0.625° longitude spatial resolution ~~are~~were used.

2.8 CAMSRA AOD reanalysis

The Copernicus Atmosphere Monitoring Service (CAMS) Reanalysis (CAMSRA, Inness et al., 2019) is a new global reanalysis of atmospheric composition produced at the ECMWF~~, after~~. It followed on the heels of the MACC reanalysis (Inness et al., 2013) and CAMS interim reanalysis (Flemming et al., 2017). The dataset covers the period of 2003–2020 and is being continued for subsequent years. The model is driven by the Integrated Forecasting System (IFS) used at ECMWF for weather forecasting and meteorological reanalysis~~,~~ (but at a coarser resolution ~~and with~~). It incorporates additional modules activated for prognostic aerosol species (dust, sea salt, organic matter, black carbon and sulfate) and trace gases. ~~Radiative~~The radiative impact of aerosol particles and ozone on meteorology is included. Satellite retrievals of total AOD at 550 nm are assimilated from MODIS for the whole period, and from the Advanced Along-Track Scanning Radiometer for 2003–2012, using a 4D variational data assimilation system with a 12-hour data assimilation window along with meteorological and trace gas observations. The speciated AOD products are available at a 3-hourly temporal resolution and a ~0.7° spatial resolution, and monthly mean AODs at 550 nm ~~are~~were used in this study. Model development has generally improved the speciation of aerosols compared with earlier reanalyses, and evaluation against AERONET globally is largely consistent over the period of the reanalysis.

2.9 Multi-reanalysis-consensus (MRC) AOD

All three of the individual reanalyses are largely independent in their underlying meteorology and in their aerosol sources, sinks, microphysics, and chemistry. They were also generated through data assimilation (DA) of satellite and/or ground-based observations of AOD. The assimilation methods, and the assimilated AOD observations, including the treatments of the observations prior to assimilation (quality control, bias correction, aggregation, and sampling, etc.), ~~are~~ often ~~different too, despite~~differ. There is, on the other hand, consistent use of ~~data from the~~ MODIS data with its daily global spatial coverage.

Based on the three aerosol reanalysis products described above, we made an MRC product following the multi-model-ensemble method of the International Cooperative for Aerosol Prediction (ICAP, Sessions et al., 2015; Xian et al., 2019). The MRC is a consensus mean of the three individual reanalyses, with a 1°x1° degree spatial and monthly temporal resolution. Speciated AODs and total AOD at 550 nm for 2003-2019 are available. This new product is validated here~~ with ground-based AERONET observations for the Arctic~~ , along with the three component reananlysis members, using ground-based Arctic AERONET observations. Validation results in terms of bias, RMSE, and coefficient of determination (r^2) for monthly-mean total, FM and CM AODs are presented in Tables 2, 3, 4. The MRC, in accordance with the ICAP multi-model-consensus evaluation result, is found to generally be the top performer among all of the reanalyses for the study region.

2.10 Fire Locating and Modeling of Burning Emissions (FLAMBE) v1.0

FLAMBE is a biomass-burning emission inventory ~~based on~~derived from a satellite-based active fire hotspot approach (Reid et al., 2009; Hyer et al., 2013). FLAMBE can take satellite fire products from either geostationary sensors, which offer faster refresh rates and observation of the full diurnal cycle, or polar orbiters, which have a greater sensitivity. There are significant daily sampling biases and additional artifacts from day to day shifts in the orbital pattern for polar-orbiting satellites (e.g., Heald et al., 2003, Hyer et al., 2013). However, the polar-only version of FLAMBE, which ~~takes~~employed MODIS-based fire data, is more appropriate for reanalysis and trend analysis~~, as over the study period,~~. This is because multiple changes in the geostationary constellation over the stud period posed a challenge ~~for consistency~~in terms of ~~the~~ smoke source-function~~. Because of the same requirement for temporal~~ consistency~~, the~~. The FLAMBE MODIS-only smoke source was also used in the NAAPS-RA v1~~. Inferring from~~ because of the same temporal consistency requirement. FLAMBE show similar BB emission trends as the time series of yearly BB emission for the Arctic region based on other inventories for a similar study period (using BC emission of Fig. 2 in McCarty et al., 2021).~~, including~~ These inventories include the Global Fire Assimilation System (GFAS;

Kaiser et al., 2012), and the Global Fire Emission Dataset (GFED; Randerson et al., 2006; van derWerf et al., 2006~~), FLAMBE has the same sign of trend of BB emissions for the similar study period (using BC emission of Fig.).~~ 2 in McCarty et al., 2021).~~

3. Method

The Arctic AOD climatology and trends are analyzed in this study using remote sensing products derived from MODIS, MISR, CALIOP, and AERONET (each sensor typically generating aerosol products of different native wavelengths). The 550 nm AOD was employed as the benchmark parameter for this study since the three aerosol reanalyses AODs and the MODIS AOD are all available at 550 nm while the 558nm and 532nm AODs of MISR and CALIOP are appreciably close to 550 nm. AERONET and MAN modal AODs at 550 nm were derived using the SDA method as described in Sect. 2.4 and 2.5. Arithmetic means were employed for all the data processing in order to be consistent with the arithmetic statistics that are usually reported in the literature and with the arithmetic statistics of the monthly data from the aerosol reanalyses. Various studies have shown that geometric statistics are more representative of AOD histograms (see, for example, Hesaraki et al., 2017 and Sayer et al., 2019). However, Hesaraki et al. (2017) showed that arithmetic statistics could be employed to readily estimate geometric statistics[1]. This option effectively renders the reporting of arithmetic or geometric statistics less critical.

The species of interest are biomass burning (BB) smoke, anthropogenic and biogenic fine aerosols (ABF) in NAAPS, and its equivalent of sulfate for MERRA-2 ~~and~~as well as CAMSRA~~,~~ and dust and sea salt aerosols. Anthropogenic aerosol particles, as an external climate forcer, ~~normally draw noticeable~~have drawn some attention in climate studies (e.g~~.~~., Wang et al., 2018; Ren et al., 2020; Yang et al., 2018; Sand et al., 2016; Eckhardt et al., 2015; Brieder et al., 2017). However, BB smoke, which can be both natural and anthropogenic in origin, ~~are often~~has been shown to be the largest contributor ~~to AOD and concentration during the Arctic summer (~~over the last two decades~~, in both modeling~~) to Arctic summer AOD and concentration (Evangeliou et al. 2016; Sand et al. 2017~~)~~ for modelling studies and ~~observational-based studies (~~Eck et al. 2009; Eckhardt et al. 2015; Stohl et al. 2007; Warneke et al. ~~2009~~2009 for observational-based studies). Recent measurements of BC in Arctic snow also show a strong association with BB based on tracer correlations and optical properties (Hegg et al., 2009; Doherty et al., 2010; Hegg et al., 2010; Khan et al., 2017). A climate modeling study recently found that ~~a~~ much larger Arctic climate variability and enhanced sea ice melting ~~are~~were introduced ~~by~~ using BB emissions with interannual variability ~~compared~~as opposed to ~~using a~~ climatological monthly~~-~~mean BB ~~emission~~emissions

[1] with an erratum: the equation (2) transformation to geometric mean should be $\tau_{g,x} = \frac{<\tau_x>}{\exp\left(\frac{\ln^2 \mu_x}{2}\right)}$)

(DeRepentigny et al., 2021), ~~indicating~~a result that underscored the importance of quantifying the magnitude and interannual variability of BB smoke in Arctic climate forcing estimates. Thus BB smoke AOD is separated out from the total AOD as a ~~single~~singularly important species in this study.

The separation of species in this analysis is a bit arbitrary ~~as~~since the representation of different aerosol types and sources in each reanalysis is slightly different. The NAAPS model is unique compared to other reanalyses and operational models in that it carries aerosol species by source rather than chemical speciation. For example, biomass burning and a combined ABF are carried as separate species and permit explicit hypothesis testing about the sources, sinks, and optical properties. Conversely, MERRA-2 and CAMSRA carry organic carbon (OC)/organic matter (OM), black carbon (BC) and various inorganic species combining a multitude of anthropogenic, biogenic and open biomass burning source pathways. In this study the sum of OC/OM and BC AOD is used to approximate BB smoke AOD from CAMSRA and MERRA-2. The ratio of BC to the sum of BC and OC/OM is about 10% for areas north of 60°N on average for both MERRA-2 and CAMSRA for both MAM and JJA~~, except~~ (the single exception to this is that the MERRA-2 ratio is about 20% in ~~MERRA-2 for~~ MAM~~.~~).

It is worth noting that all the three reanalyses use hourly/daily BB smoke emission inventories that use dynamic smoke sources detected by polar-orbiting satellites~~, e.g.,~~. Examples include FLAMBE (Reid et al., 2009) for NAAPS-RA, Quick Fire Emissions Dataset (QFED) for MERRA-2 after 2010 (GFED with monthly BB emission before 2010, Randerson et al., 2006; van derWerf et al., 2006), and Global Fire Assimilation System (GFAS, Kaiser et al., 2012) for CAMSRA. This is expected to yield a better spatial and temporal representation of BB smoke emissions compared to ~~the~~ climate models ~~in~~ which use monthly mean BB inventories ~~are often applied~~ (e.g~~.~~., Sand et al., 2017).

We also assume all dust and sea salt are CM, while other model aerosol species, including ABF in NAAPS-RA, sulfate in MERRA-2 and CAMSRA, BB smoke in NAAPS-RA, black carbon and organic carbon in MERRA-2 and CAMSRA are FM aerosol particles. This approximation (the sequestering of dust and sea salt to the coarse mode regime) is based on the fact that FM dust and sea salt only contribute ~~to~~ a small portion of the total dust or sea salt AOD at 550 nm ~~(for~~. For example, FM mode dust ~~contributes to~~represents about 30% and 39% of total dust AOD globally in MERRA-2 and CAMSRA respectively. The numbers are 17% and 10% for sea salt~~), while~~. While NAAPS-RA ~~has a simple microphysics~~makes the simplifying microphysical assumption that ~~assumes~~ all dust and sea salt are CM. This usage renders the FM and CM bulk-aerosol ~~analysis~~comparisons more ~~convenient.~~tractable (with the rider that we must remain

conscious of any artificial separation that might be created by any FM or CM oversimplification).

The significance test for trend analysis applies the same calculation method as in Zhang et al. (2010; 2017), ~~following~~an approach which, in turn, was based on the method of Weatherhead et al. (1998). This trend analysis method requires a continuous time series of data.

4. Comparison of AODs from aerosol reanalyses and AERONET

The number of AERONET observations are ~~typically more frequent~~tied to the increase in the number of daylight hours and are therefore more numerous during the summer than in the spring ~~and are therefore more~~ . This translates to their generally being more temporally representative of 6 hr or daily means in JJA. As a consequence, we preferentially used a JJA climatology to illustrate reanalyses vs AERONET comparisons. Fig. ~~Figure~~ 1 shows the 2003-2019 ~~JJA~~ mean ~~fine mode (~~JJA FM~~)~~ and ~~coarse mode (~~CM~~)~~ AODs ~~at 550 nm~~ from AERONET and the speciated AODs ~~at 550 nm~~ from NAAPS-RA, MERRA-2, and CAMSRA~~.~~ (all at 550 nm). All three aerosol reanalyses appear to capture the total AOD magnitudes to varying extents. The AERONET retrievals show that total AOD during the Arctic JJA season is dominated by contributions from FM aerosols. ~~High~~Large FM AOD values (generally indicative of strong BB smoke influence) are found in Yakutsk and Tiksi in Siberia, and Bonanza Creek in Alaska. CM aerosols also contribute a substantial fraction, varying from a minimum of 15% in regions close to BB smoke sources to a maximum of ~25% at the Norwegian Sea and Greenland Sea coastal sites (Hornsund, Andenes, and Ittoqqortoormitt): these sites are likely impacted by sea salt aerosols lifted by North Atlantic cyclonic events. NAAPS-RA produces AERONET-comparable FM and total AODs in general while showing a tendency to overestimate CM AODs (see Table 2 for explicit biases). The other two reanalyses (MERRA-2 and CAMSRA) produce higher FM AOD and total AOD and lower CM AOD compared to AERONET (see also Table 2).

Differences exist between the three reanalyses with respect to the FM and CM partitioning of aerosol species. For example, sea salt aerosols always dominate in the CAMSRA (dust + sea salt) CM: this ~~is a~~ comment ~~that~~ even applies to some inland sites (e.g. ~~.~~ .. Bonanza-Creek) and implies a modeling issue. Dust is the dominant CM species in NAAPS-RA and MERRA-2. This latter result was found ~~for~~at all AERONET ~~sites~~site positions: it is likely attributable to elevated dust layers transported from lower latitudes (Stone et al, 2007; Jacob et al., 2010; Breider et al., 2014; Aboele-Fetouh et al., 2020). The proportional contribution of dust to total AOD is the largest in NAAPS-RA: a result that could have contributed to its high bias in CM AOD (Table 2). The contribution of organic matter to FM AOD is generally larger in CAMSRA than in the other two

reanalyses. On the whole, BB smoke is the largest contributing species to total JJA AOD over the Arctic. This is consistent across all the reanalyses except for some sites in NAAPS-RA (e.g. Andenes, Hornsund, and Kangerlussuaq where ABF AOD is slightly larger than BB smoke AOD). This can be partially due to the different types of speciation employed in NAAPS-RA: ABF includes anthropogenic and biogenic pollution aerosols, including sulfate, BC and organic aerosols of all origins (except for biomass burning aerosols). It is also worth noting that mean AERONET AODs ~~over these Arctic sites~~ are, in general, higher (0.01-0.02, and can be ~0.1 higher for the sites close to BB sources) than their median counterparts (Table 1) as well as their geometric means. This is because AOD histograms are typically more lognormal than normal in form (asymmetric linear-AOD histograms with positively skewed tails as per, for example, Hesaraki et al., 2017): arithmetic means are, accordingly, often driven by extreme (>95% percentile for example) AOD events. Because these extreme events constitute an important part of the Arctic aerosol environment, the AOD means are presented here.

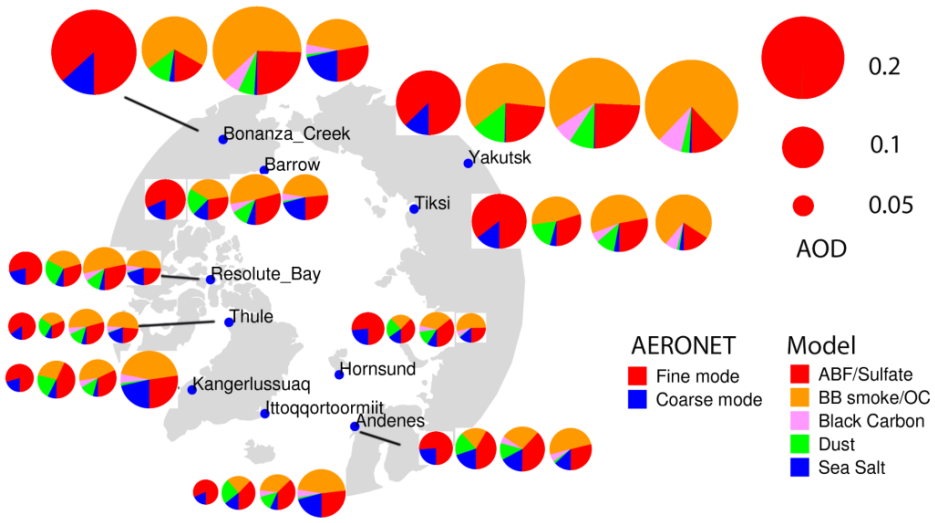

Figure 1. Polar projection map showing the locations of the AERONET Arctic sites (small solid blue ~~dots~~circles) used in this study. Long-term (2003-2019) JJA-mean FM and CM AODs at 550 nm from AERONET (leftmost circle of each group of four circles) and respectively, the speciated pie-charts of 550 nm AODs from NAAPS-RA, MERRA2, and CAMSRA for each site. Warm colors (red, orange, and pink) represent fine mode and cool colors (green and blue) represent coarse mode.

Table 1. Geographical ~~properties~~coordinates of AERONET sites used in this study, and seasonal mean total~~,~~ and SDA-derived FM and CM AOD at 550nm ~~derived with SDA~~ for MAM and JJA based on 2003-2019 data when available. "n" represents the number of 6-hrly AERONET data.

sites	latitude	longitude	elev (m)	region	MAM (mean|median|std)				MAM FMF		JJA (mean|median|std)				JJA FMF	
					total AOD	FM AOD	CM AOD	n	mean	median	total AOD	FM AOD	CM AOD	n	mean	median
Hornsund	77.0°N	15.6°E	12	Svalbard	0.10|0.09|0.05	0.07|0.06|0.04	0.03|0.02|0.03	846	0.71	0.75	0.08|0.06|0.07	0.06|0.04|0.07	0.02|0.01|0.02	971	0.77	0.83
Thule	76.5°N	68.8°W	225	Greenland	0.08|0.07|0.05	0.06|0.05|0.03	0.03|0.01|0.04	1,009	0.75	0.81	0.07|0.05|0.07	0.06|0.04|0.06	0.01|0.01|0.02	1,509	0.85	0.88
Kangerlussuaq	67.0°N	50.6°W	320	Greenland	0.07|0.06|0.04	0.05|0.04|0.02	0.02|0.02|0.03	957	0.69	0.72	0.07|0.05|0.05	0.05|0.04|0.05	0.01|0.01|0.02	1,768	0.77	0.78
Ittoqqortoormiit	70.5°N	21.0°W	68	Greenland	0.06|0.05|0.04	0.04|0.04|0.02	0.02|0.01|0.03	545	0.72	0.78	0.06|0.04|0.04	0.05|0.03|0.05	0.01|0.01|0.02	1,280	0.80	0.81
Andenes	69.3°N	16.0°E	379	Norway	0.08|0.07|0.05	0.05|0.04|0.03	0.03|0.02|0.03	821	0.67	0.71	0.08|0.07|0.05	0.06|0.05|0.05	0.02|0.01|0.02	1,008	0.75	0.78
Resolute_Bay	74.7°N	94.9°W	35	Nunavut	0.10|0.08|0.05	0.07|0.06|0.04	0.03|0.02|0.03	520	0.73	0.78	0.08|0.05|0.10	0.06|0.04|0.10	0.02|0.01|0.03	1,178	0.78	0.83
Barrow	71.3°N	156.7°W	8	Alaska	0.11|0.09|0.07	0.08|0.06|0.05	0.03|0.02|0.04	605	0.73	0.77	0.10|0.07|0.15	0.08|0.05|0.15	0.02|0.01|0.02	1,155	0.79	0.82
Bonanza_Creek	64.7°N	148.3°W	353	Alaska	0.10|0.08|0.09	0.06|0.04|0.08	0.04|0.03|0.04	953	0.61	0.60	0.21|0.09|0.36	0.18|0.06|0.35	0.03|0.02|0.03	1,717	0.75	0.76
Tiksi	71.6°N	129.0°E	17	Siberia	0.10|0.10|0.03	0.08|0.08|0.03	0.02|0.01|0.02	39	0.80	0.82	0.13|0.08|0.18	0.11|0.07|0.17	0.02|0.01|0.02	449	0.80	0.85
Yakutsk	61.7°N	129.4°E	119	Siberia	0.15|0.11|0.15	0.11|0.08|0.13	0.04|0.02|0.04	1,516	0.76	0.80	0.16|0.09|0.24	0.14|0.07|0.24	0.02|0.01|0.02	2,579	0.81	0.84
MAN	>70°N	-		Arctic Ocean	0.11|0.10|0.06	0.06|0.06|0.04	0.04|0.04|0.03	85	0.62	0.62	0.06|0.05|0.07	0.04|0.03|0.07	0.02|0.02|0.01	435	0.66	0.67

Table 1 provides ~~detailed~~the geographical ~~properties~~coordinates of the ten AERONET sites and the (arithmetic) mean, median and standard deviation of total, FM and CM AODs at 550 nm for both MAM and JJA based on available 2003-2019 data (the availability of AERONET data can be ~~inferred~~appreciated from the monthly time series in ~~Figure 2).~~Fig. 2). Analogous MAN statistics are provided in the last row of Table 1 (see also Fig. S1 for geographical distributions of MAN measurements). The seasonal mean total AOD for Resolute Bay, the Greenland sites ~~and~~, Hornsund ~~sites~~and the MAN measurements are < ~ 0.1 (0.06-0.10) while the Alaskan and Siberian ~~sites~~site values are >~ 0.1 (0.10 to 0.15 with Bonanza Creek displaying a substantially larger JJA value of 0.21 ~~in JJA~~). All sites, except Bonanza Creek, tend to have moderately higher median AOD in MAM: this is consistent with other Arctic sunphotometer studies (Tomasi et al., 2015; Xie et al., 2018). The JJA decrease ~~in JJA~~, according to the reanalyses (Fig. 4 and 5), is related to higher FM ABF/sulfate and/or CM dust and sea salt in MAM. ~~It is also noted that this~~This AOD seasonal difference may have evolved in the past two decades with a decreasing trend in ABF/sulfate as discussed in Sect. 5.3. The seasonal mean AOD is greater in JJA than in MAM for Yakutsk, Tiksi and Bonanza Creek: this is likely due to strong FM AOD variations associated with BB smoke events (see, for example, the discussions concerning the seasonal competition between FM AOD smoke and FM AOD Arctic haze, in AboEl-Fetouh et al., 2020). The standard deviations of the total and FM AODs are also high for those three sites.

The Table 1 median and mean of the FMF vary, respectively, between 0.60 to 0.88 and 0.~~66~~61 to 0.85 with higher FMF in JJA than in MAM. The MAM to JJA increase is coherent with the month-to-month increase of AboEl-Fetouh et al., (2020) although their 550 nm arithmetic means tend to be larger (monthly-binned extremes of 0.81 to 0.98). ~~Most~~Most, or at least a significant part of this difference is likely attributable to differences between our FMF (SDA) separation of the product and the SMF

(AERONET-inversion) separation of AboEl-Fetouh et al.'s climatology: the SMF is generally larger than the FMF because it tends to attribute a fraction of the CM particle size distribution and thus a fraction of the CM AOD to the FM AOD -(see, for example, the 550 nm SMF vs FMF comparisons Section 4 of Kleidman et al., 2005). More discussions about the differences in terms of FMF vs. SMF and arithmetic vs. geometric statistics are available in the supplement material.

Table 2. Total, FM and CM AOD bias of CAMSRA, MERRA-2, NAAPS-RA and their consensus mean MRC compared to AERONET monthly data.

sites	Bias-total AOD				Bias-FM AOD				Bias-CM AOD			
	CAMSRA	MERRA2	NAAPS-RA	MRC	CAMSRA	MERRA2	NAAPS-RA	MRC	CAMSRA	MERRA2	NAAPS-RA	MRC
Hornsund	-0.02	0.01	0.00	0.00	-0.01	0.01	-0.01	0.00	-0.01	0.01	0.02	0.00
Thule	0.00	0.02	0.00	0.01	0.01	0.02	-0.01	0.01	-0.01	0.00	0.01	0.00
Kangerlussuaq	0.02	0.02	0.02	0.02	0.03	0.02	0.02	0.02	-0.01	0.00	0.02	0.00
Ittoqqortoormiit	0.04	0.03	0.02	0.03	0.04	0.02	0.00	0.02	0.00	0.01	0.02	0.01
Andenes	0.03	0.04	0.02	0.03	0.03	0.02	0.00	0.02	0.00	0.02	0.02	0.01
Resolute_Bay	0.01	0.02	0.01	0.01	0.03	0.02	0.00	0.02	-0.02	0.00	0.01	0.00
Barrow	0.02	0.03	0.00	0.02	0.04	0.03	-0.01	0.02	-0.02	0.00	0.02	0.00
Bonanza_Creek	0.06	0.04	0.00	0.03	0.09	0.05	0.00	0.05	-0.02	-0.01	0.00	-0.01
Tiksi	0.02	0.02	-0.01	0.01	0.04	0.02	-0.01	0.02	-0.02	0.00	0.01	0.00
Yakutsk	0.03	0.04	0.01	0.03	0.05	0.05	0.00	0.03	-0.02	0.00	0.01	-0.01
mean	0.02	0.03	0.01	0.02	0.04	0.03	0.00	0.02	-0.01	0.00	0.01	0.00
median	0.02	0.03	0.01	0.02	0.04	0.02	0.00	0.02	-0.02	0.00	0.02	0.00

Table 3. Same as Table 2, except for RMSE.

sites	RMSE-total AOD				RMSE-FM AOD				RMSE-CM AOD			
	CAMSRA	MERRA2	NAAPS-RA	MRC	CAMSRA	MERRA2	NAAPS-RA	MRC	CAMSRA	MERRA2	NAAPS-RA	MRC
Hornsund	0.04	0.02	0.02	0.02	0.03	0.02	0.02	0.02	0.02	0.01	0.02	0.01
Thule	0.02	0.03	0.02	0.02	0.03	0.03	0.02	0.02	0.02	0.01	0.02	0.01
Kangerlussuaq	0.03	0.03	0.03	0.03	0.04	0.02	0.02	0.02	0.01	0.01	0.02	0.01
Ittoqqortoormiit	0.04	0.03	0.02	0.03	0.05	0.03	0.01	0.02	0.01	0.01	0.02	0.01
Andenes	0.03	0.04	0.03	0.03	0.03	0.03	0.02	0.02	0.01	0.02	0.03	0.02
Resolute_Bay	0.03	0.04	0.02	0.03	0.04	0.04	0.02	0.03	0.02	0.01	0.02	0.01
Barrow	0.05	0.05	0.03	0.04	0.06	0.04	0.03	0.03	0.02	0.01	0.02	0.01
Bonanza_Creek	0.11	0.10	0.07	0.08	0.12	0.10	0.06	0.08	0.03	0.02	0.01	0.02
Tiksi	0.05	0.04	0.02	0.03	0.06	0.04	0.02	0.03	0.02	0.01	0.01	0.01
Yakutsk	0.07	0.07	0.04	0.06	0.08	0.07	0.04	0.06	0.03	0.01	0.01	0.01
mean	0.05	0.05	0.03	0.04	0.05	0.04	0.03	0.03	0.02	0.01	0.02	0.01
median	0.04	0.04	0.03	0.03	0.05	0.04	0.02	0.03	0.02	0.01	0.02	0.01

Table 4. Same as Table 2, except for r^2.

sites	r2-total AOD				r2-FM AOD				r2-CM AOD			
	CAMSRA	MERRA2	NAAPS-RA	MRC	CAMSRA	MERRA2	NAAPS-RA	MRC	CAMSRA	MERRA2	NAAPS-RA	MRC
Hornsund	0.23	0.78	0.75	0.73	0.35	0.73	0.71	0.67	0.27	0.45	0.55	0.56
Thule	0.50	0.47	0.73	0.64	0.52	0.45	0.70	0.62	0.01	0.26	0.44	0.41
Kangerlussuaq	0.48	0.54	0.42	0.53	0.52	0.52	0.35	0.52	0.00	0.57	0.16	0.35
Ittoqqortoormiit	0.68	0.75	0.67	0.79	0.63	0.81	0.76	0.83	0.24	0.36	0.14	0.35
Andenes	0.67	0.63	0.68	0.71	0.68	0.66	0.64	0.71	0.10	0.23	0.21	0.21
Resolute_Bay	0.52	0.51	0.67	0.63	0.53	0.49	0.73	0.62	0.02	0.06	0.03	0.05
Barrow	0.33	0.68	0.70	0.62	0.45	0.76	0.69	0.68	0.05	0.27	0.41	0.41
Bonanza_Creek	0.81	0.78	0.80	0.83	0.83	0.79	0.82	0.85	0.06	0.43	0.45	0.46
Tiksi	0.77	0.80	0.87	0.84	0.82	0.82	0.90	0.86	0.02	0.20	0.10	0.15
Yakutsk	0.70	0.70	0.80	0.77	0.78	0.71	0.80	0.80	0.01	0.41	0.42	0.42
mean	0.57	0.66	0.71	0.71	0.61	0.67	0.71	0.72	0.08	0.32	0.29	0.34
median	0.60	0.69	0.72	0.72	0.58	0.72	0.72	0.70	0.04	0.32	0.31	0.38

584

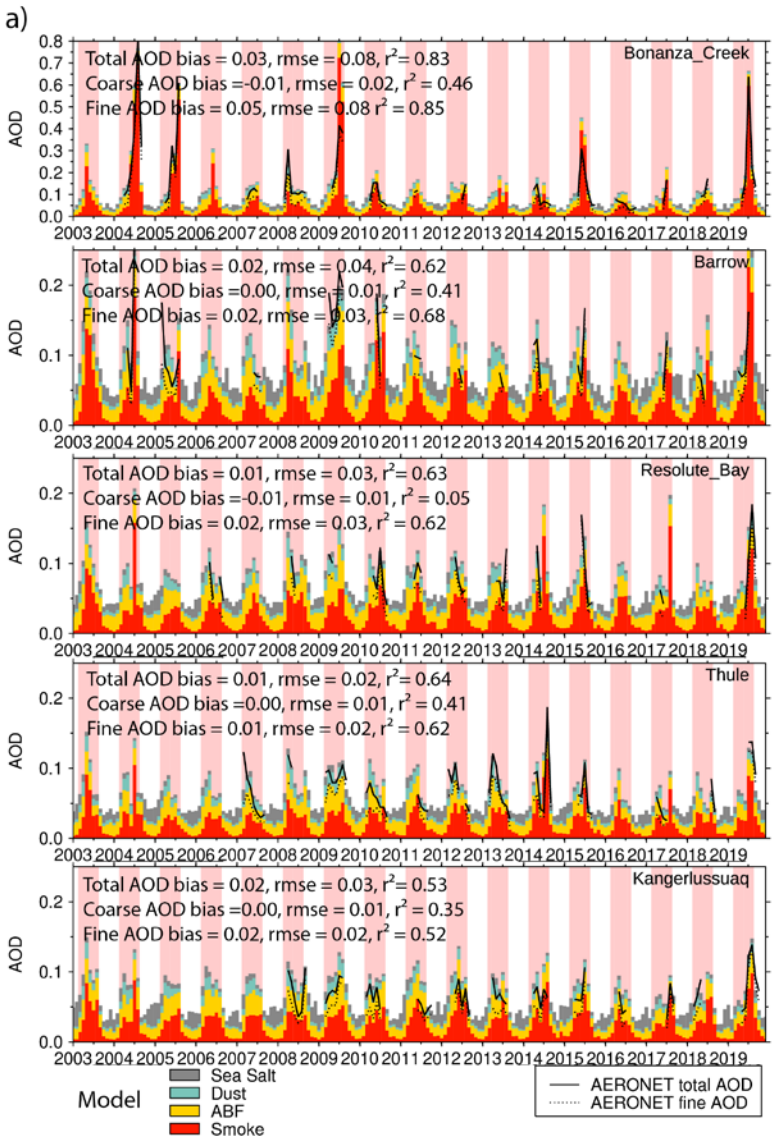
a)
Bonanza_Creek
Total AOD bias = 0.03, rmse = 0.08, r²= 0.83
Coarse AOD bias =-0.01, rmse = 0.02, r² = 0.46
Fine AOD bias = 0.05, rmse = 0.08 r² = 0.85
Barrow
Total AOD bias = 0.02, rmse = 0.04, r²= 0.62
Coarse AOD bias =0.00, rmse = 0.01, r² = 0.41
Fine AOD bias = 0.02, rmse = 0.03, r² = 0.68
Resolute_Bay
Total AOD bias = 0.01, rmse = 0.03, r²= 0.63
Coarse AOD bias =-0.01, rmse = 0.01, r² = 0.05
Fine AOD bias = 0.02, rmse = 0.03, r² = 0.62
Thule
Total AOD bias = 0.01, rmse = 0.02, r²= 0.64
Coarse AOD bias =0.00, rmse = 0.01, r² = 0.41
Fine AOD bias = 0.01, rmse = 0.02, r² = 0.62
Kangerlussuaq
Total AOD bias = 0.02, rmse = 0.03, r²= 0.53
Coarse AOD bias =0.00, rmse = 0.01, r² = 0.35
Fine AOD bias = 0.02, rmse = 0.02, r² = 0.52
AOD
2003 2004 2005 2006 2007 2008 2009 2010 2011 2012 2013 2014 2015 2016 2017 2018 2019
Model
Sea Salt
Dust
ABF
Smoke
AERONET total AOD
AERONET fine AOD

585

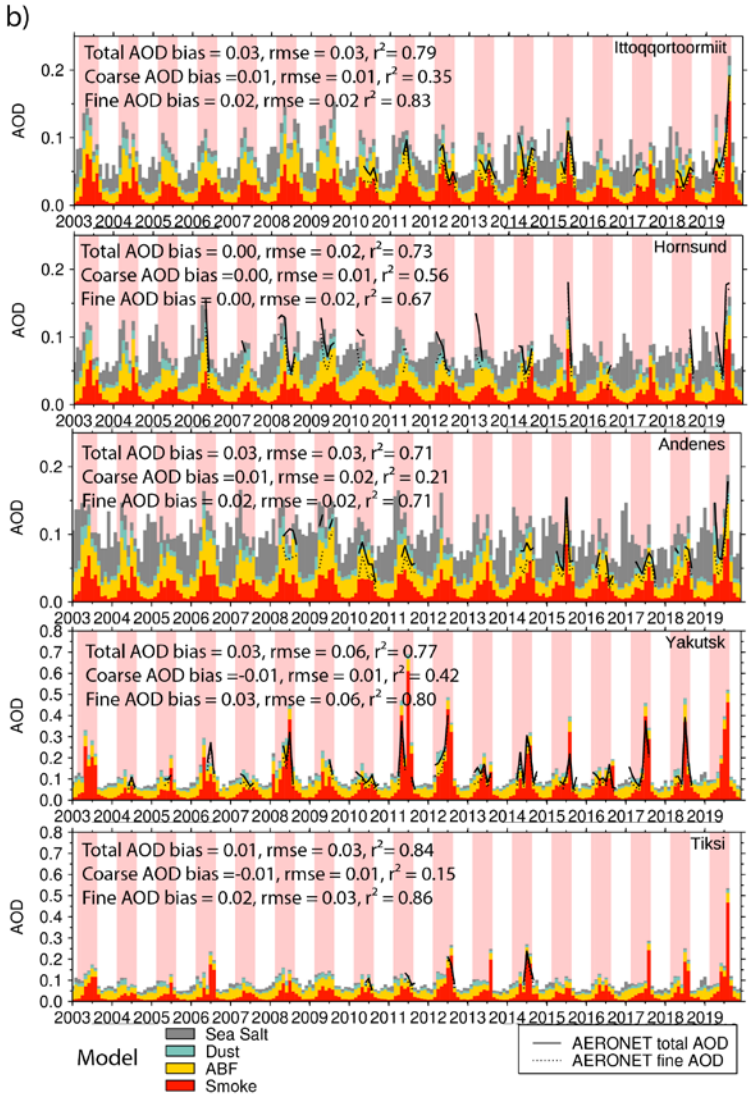

Figure 2. Monthly time series of ~~fine, coarse~~FM, CM, and total ~~AODs from~~ AERONET AODs and MRC speciated AOD at a) Bonanza Creek, Barrow, Resolute_Bay, Thule, Kangerlussuq, and b) Ittoqqortoormitt, Hornsund, Andenes, Yakutsk, and Tiksi sites. The JJA periods are highlighted with pink shading for easy reading. ~~Annotations for~~ The legends of each time series show MRC bias, RMSE and r^2 ~~calculated from the MRC.~~.

Monthly mean AERONET ~~AOD~~AODs is obtained only when the total number of 6-hr ~~AERONET~~ data exceeds 18 to ensure temporal representativeness.

Fig.~~Figure~~ 2 shows the time series of monthly mean ~~modal AODs~~FM, CM and total AODs from the ~~10~~ten AERONET stations (CM AOD can be inferred from the difference between total AOD and FM AOD) and the speciated AODs from MRC (recall the approximation of assigning dust and sea salt ~~as~~to the CM, and ABF/sulfate and smoke ~~as~~to the FM). The MRC monthly-binned verification statistics at the ten AERONET sites ~~based on monthly data~~ are given in the Fig. 2 legends ~~of Figure 2~~. Verification statistics of individual aerosol reanalysis members and the MRC based on monthly data are presented in Tables 2, 3, and 4 for bias, RMSE, and r^2 respectively. The MRC is consistently biased slightly high for FM AOD across all sites and about neutral for CM AOD for most. As a result, total AOD tends to bias slightly high, with biases ranging from 0.00 to 0.03. RMSE values range from 0.02 to 0.03 for most sites, except for Bonanza Creek, Yakutsk and Barrow with RMSE values of 0.06, 0.05 and 0.04~~,~~ (driven mainly by FM variations~~.~~). The r^2 ~~value ranges~~values range from 0.53 to 0.84, with FM AOD ~~correlation~~r^2 values ranging from much higher to marginally higher than ~~that of~~the CM AOD values. This is understandable as FM AOD displays large variabilities (which models are more capable of capturing) while CM AOD displays relatively low values and smaller absolute variabilities on seasonal and interannual time scales. Also, emissions of CM aerosols like dust and sea salt, are driven dynamically by model or reanalysis surface winds where the surface wind dependency increases exponentially in amplitude: the simulation of this dependency has been a challenge to all global aerosol models (Sessions et al., 2015; Xian et al., 2019).

Our previous experience with multi-reanalysis and multi-model ensembles indicates, in general, that the consensus of multi-reanalyses or multi-models show better verification scores than individual component members (Sessions et al., 2015; Xian et al., 2019; Xian et al., 2020). However, these studies are based on more global analyses for which the Arctic impact is relatively weak because of the sparsity of observational Arctic data. Tables 2, 3 and 4 indicate that the Arctic is rather unique inasmuch as the MRC is not necessarily the top AOD-estimation performer. NAAPS-RA generally has moderately better bias, RMSE and r^2 verification scores for the total and FM AODs compared to MERRA-2 and CAMSRA while CM AOD does not perform as well. In previous MRC and multi-model consensus evaluations, all component members either performed comparably in terms of AOD RMSE, bias and r^2 or the number of multi models was relatively larger (e.g~~.~~., 5 to 6 for the International Cooperative for Aerosol Prediction multi-model consensus). This study is the first time that all three developing centers have systematically evaluated their AOD reanalysis performance on an Arctic-wide climate scale.

5. ~~Results of Arctic AOD climatology, trend and extreme event statistics~~Seasonal Analysis

In this section we present spring and summertime Arctic AOD climatologies derived from space-borne remote sensing retrievals and aerosol reanalyses. We then present the seasonal cycle, interannual variability and trends of total and speciated AODs. ~~Statistics of extreme AOD events in the Arctic are provided in the end.~~

5.1 Spring and Summertime AOD Climatology for the Arctic

5.1.1 Space-based remote sensing AOD climatology

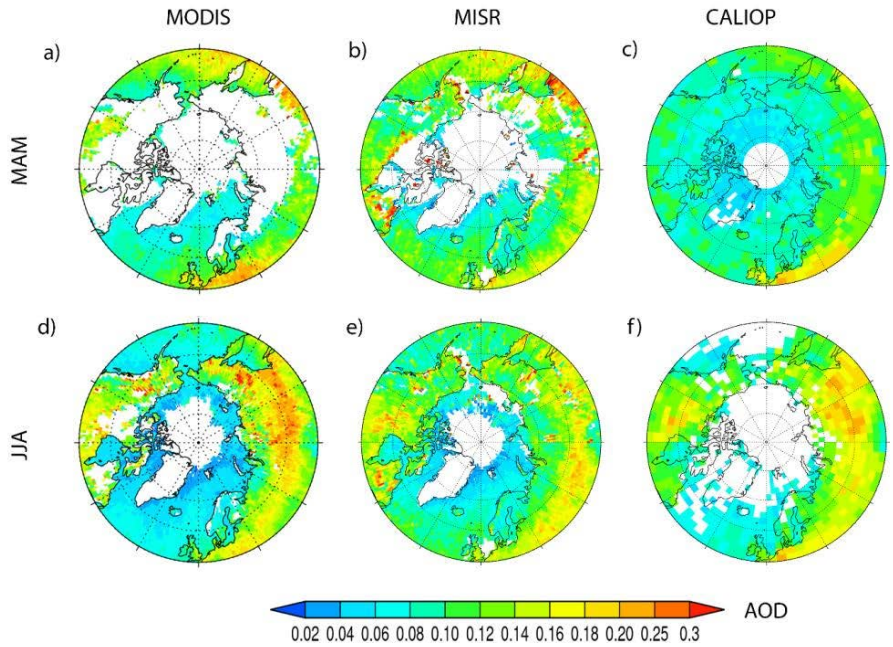

Figure 3. Satellite-derived, mean climatological MAM (upper) and JJA (lower) MODIS AOD at 550 nm (left), MISR AOD at 558 nm (middle), and CALIOP AOD at 532 nm (2006-2019, right). These are based on MODIS C6 DT+DB and MISR AOD v23 over 2003-2019, and CALIOP AOD over 2006-2019. White area means lack of data.

Bright, snow- and ice-covered surfaces, large solar zenith angles (SZA) (to the extreme of sub-horizon SZAs during the polar night), and extensive cloud coverage result in limited (quality assured) Arctic aerosol retrievals by passive-based sensors like MODIS and MISR. The latitude limit of an active, downward-looking, polar-orbiting sensor like CALIOP

on CALIPSO results in a polar region profile gap above 82°N. Known issues of CALIOP with retrieval filled values (RFVs) (Toth et al., 2018) and high noise to signal ratio over the Arctic also limit its aerosol retrievals near the Arctic. These challenges are reflected as no data coverage (Fig. 3) in the high Arctic and Greenland, and over large regions of North America and Siberia in both March-April-May (MAM) and June-July-August (JJA) in the AOD climatology maps based on MODIS, MISR, and CALIOP. Compared to MAM, JJA has larger data coverage from MODIS and MISR over higher latitudes as aerosol retrievals from MODIS and MISR are based on reflected sunlight. Also, when snow and sea ice melt in summer, darker ocean and land surfaces that are suitable for applying passive-based aerosol retrieval methods are exposed. MAM data coverage for CALIOP is more than that of JJA due to less solar contamination during the night than during daytime for lidars. Nevertheless, the long operation time of these sensors (about two decades) provides sufficient data to construct a climatology for the near Arctic and the midlatitude where most sources of Arctic aerosols reside.

In general, the AOD patterns from the three sensors are similar. High AODs of 0.15-0.25 appear in the 50°N-65°N latitude belt over land, i.e., large areas of boreal and subarctic Siberia, east and central Europe and North America sector in both spring and summer, with AOD mostly higher than 0.2 over Siberia in JJA, associated with biomass burning events (Fig. 3). The average AOD over water is considerably lower, ranging from 0.02 to 0.12, with relatively high AOD in the northeast Pacific influenced by outflows from the Eurasian Continent, and lower AOD over the north Atlantic, and the lowest (0.02-0.06) over the Arctic Ocean. It is also visible that AOD over water is slightly higher in MAM than in JJA, which is consistent with other observation-based studies within the Arctic circle (e.g., Tomasi et al., 2015), possibly related to higher pollution levels from the upstream continents in MAM. CALIOP AOD exhibits a similar spatial pattern as MODIS and MISR. Additionally, AOD over Greenland is on the order of 0.02-0.06, and is a minimum compared to other regions due to its high elevations (nearly 2km on average). AOD over Siberia and North America is distinctively higher in JJA than in MAM based on CALIOP. This seasonal difference can also be seen with MISR and can be explained by seasonal boreal fire activities, i.e., boreal fire is generally more active in JJA than in MAM (Giglio et al., 2013). The seemingly larger seasonal difference in CALIOP than in MODIS and MISR over Siberia and North American could also be associated with different averaging times (2006-2019 vs. 2003-2019, and ~~figure~~Fig. 2) as well as data sampling rate, as the swath for MODIS and MISR is on the order of a few hundred to a few thousand kilometers, while the swath for CALIPSO is on the order of 70m (see e.g., Colarco et al., 2014).

5.1.2 Arctic AOD climatology derived from aerosol reanalyses

~~Figure~~Fig. 4 and 5 show spatial distributions of 2003-2019 mean total and speciated AOD from the three aerosol reanalyses and their consensus mean for spring and

summer respectively. Although there is limited AOD data available for DA in the Arctic, lower latitude aerosols, whose AOD is constrained with DA, can affect Arctic AOD through transport and thus exert an indirect AOD constraint there. Additionally, all the reanalyses use satellite-fire-hotspot-based BB emissions with fine temporal resolution (hourly to daily), which exert a source constraint, especially temporally (emission magnitude differs more than timing among the different models). As a result, there are good similarities in spatial distributions of total AODs among the three reanalyses. For example, AOD values are high in the 50°N-65°N belt over the Eurasia continent and its downwind Pacific region (0.16-0.30), low and on the order of 0.1 or less for regions north of 70°N, and at a minimum over Greenland for MAM. The high AODs over boreal North America and Siberia BB regions are more prominent in JJA compared to MAM. In general, the distribution patterns and magnitude of total AOD are comparable to those derived from MODIS, MISR, and CALIOP where available to a large extent.

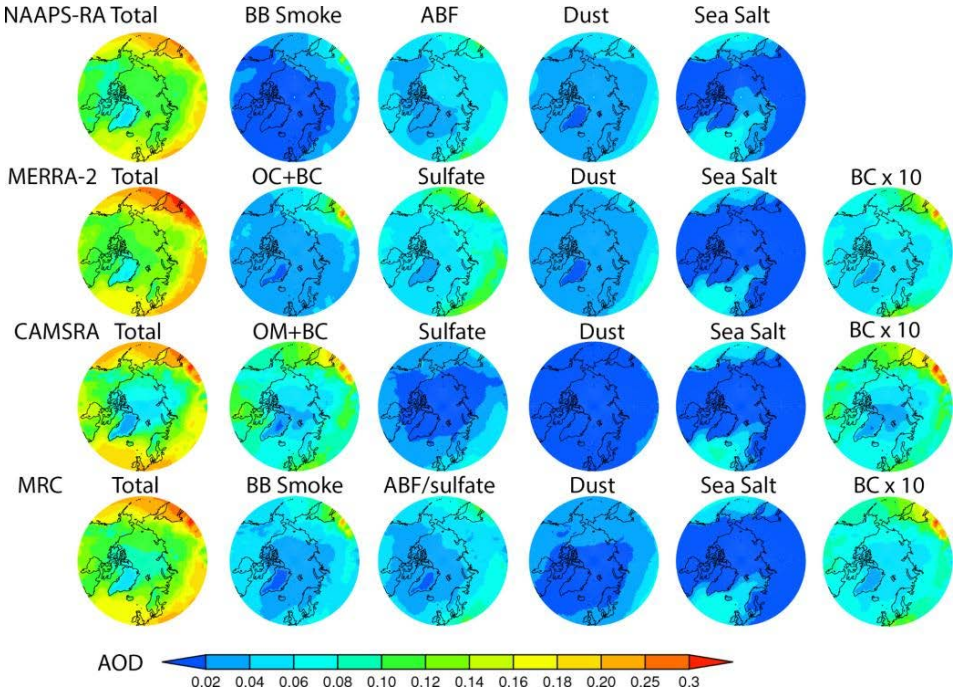

Figure 4. 2003-2019 Climatological MAM-mean total and speciated AOD at 550 nm from NAAPS-RA, MERRA-2 and CAMSRA over the Arctic. As MERRA2 and CAMSRA do not have a biomass-burning-induced single aerosol species, the sum of the organic carbon (OC)/organic matter (OM) and black carbon (BC) AODs is used to approximate biomass-burning smoke AOD. The ratio of BC to the sum of BC and OC/OM in MAM for

area >60°N is about 18% for MERRA-2 and 10% for CAMSRA. The ratios change little for area >70°N and area >80°N.

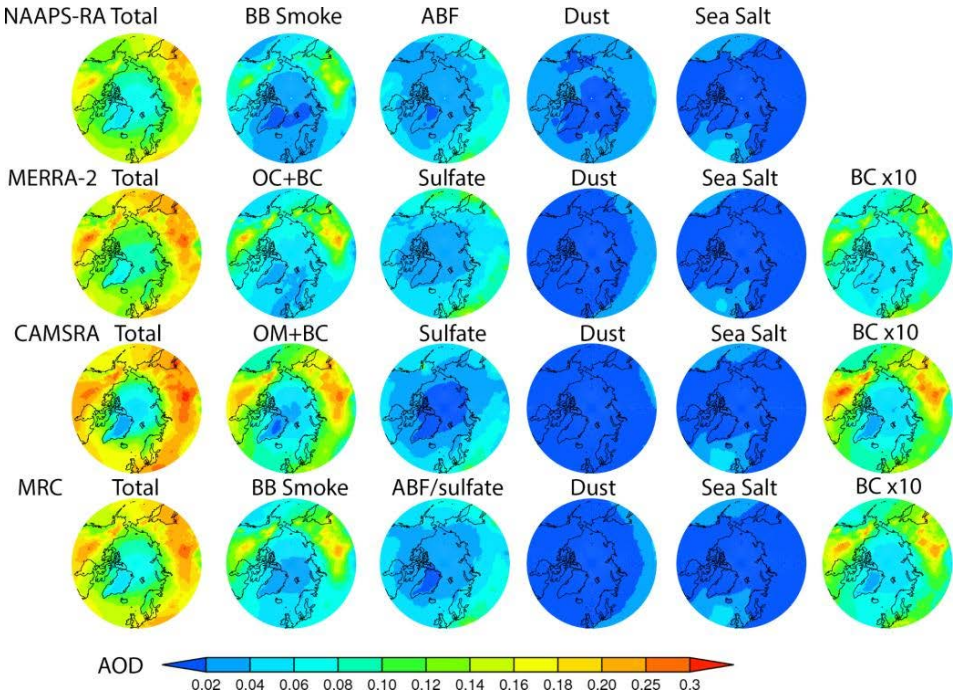

Figure 5. Same as Figure 4, except for JJA. The ratio of BC to the sum of BC and OC/OM in JJA is between 10%-11% for area >60°N for both MERRA2 and CAMSRA. This ratio changes little for area >70°N and area >80°N.

Speciated AODs have more variability than total AOD among the three reanalyses, and a little more so for MAM than for JJA (Fig. 4, 5, 6). This is understandable because passive retrievals of AOD are more available in summer than in spring near the Arctic, and therefore reanalyses have more observational constraints in summer. While total AOD is constrained through data assimilation, however, speciated AOD is not and models must rely on their physics and boundary conditions. The MRC shows that BB smoke and ABF/sulfate are similar in magnitude for the Arctic in MAM. However, by model, NAAPS-RA and MERRA-2 suggest the dominance of ABF/sulfate over BB smoke, and the reverse for CAMSRA. Based on the high bias of FM AOD verified with AERONET (Sect. 4, Table 2), CAMSRA possibly overestimates OC and BC, and hence BB smoke. BB smoke becomes the dominant species in JJA as boreal BB activity increases in summer on average and ABF/sulfate turns to the 2nd place overall. The

strengthening of smoke AOD from spring to summer is a consistent feature across all the reanalyses despite that CAMSRA tends to have higher BB smoke AOD and lower sulfate AOD compared to the other two reanalyses in both seasons. ABF/sulfate AOD level is slightly higher in MAM than in JJA for MRC (from slightly less than 0.04 to about 0.03 for 60-90°N regional average). A June minimum in total AOD is apparent from all reanalyses, associated with a general decrease in ABF/sulfate, dust and sea salt AODs after springtime and before severe BB activities in July and August. The spatial distributions of seasonal mean BC AOD from MERRA-2 and CAMSRA greatly resemble those of smoke AOD, and more so for JJA than MAM, except over Europe. This suggests a dominant role of the BB source over the anthropogenic sources of BC AOD over the Arctic for spring and summer seasons. This also supports McCarty et al. (2021)'s BC emission estimate that wildfire emissions account for more than half of all BC emissions north of ~~60N~~60°N yearly (noting much lower BB emissions during wintertime when anthropogenic BC emission is at its maximum).

For both seasons, dust and sea salt are secondary contributors to the total AOD in the Arctic, except for the noticeable influences of Saharan and Asian dust in spring (Stone et al., 2007; Brieder et al., 2014) and of sea salt in the North Atlantic, Greenland Sea, Norwegian Sea, and North Pacific associated with cyclonic activities, especially in spring. It is also noteworthy that dust AOD in CAMSRA is much lower than the other two models (<0.02) in the spring.

From the 10-degree zonal average, it is also seen that monthly and regional mean AOD gradually decreases from lower latitudinal belts to higher latitudinal belts (Fig. 7). Total AOD for the 60°-70°N belt, on average, increases from MAM to JJA due to the seasonality of BB activities. However, the total AOD for the 80~~-~~°~~-~~90°N belt decreases slightly from MAM to JJA. This means the latitudinal gradient of total AOD is larger in JJA than in MAM, which is most likely due to more wet removal of aerosols during transport from source regions to the high Arctic in summer (Garrett et al., 2010, 2011). It is also noted that the latitudinal gradient of AOD from CAMSRA is larger than those from the two other reanalyses, suggesting stronger aerosol removal in the Arctic in CAMSRA compared to MERRA-2 and NAAPS-RA.

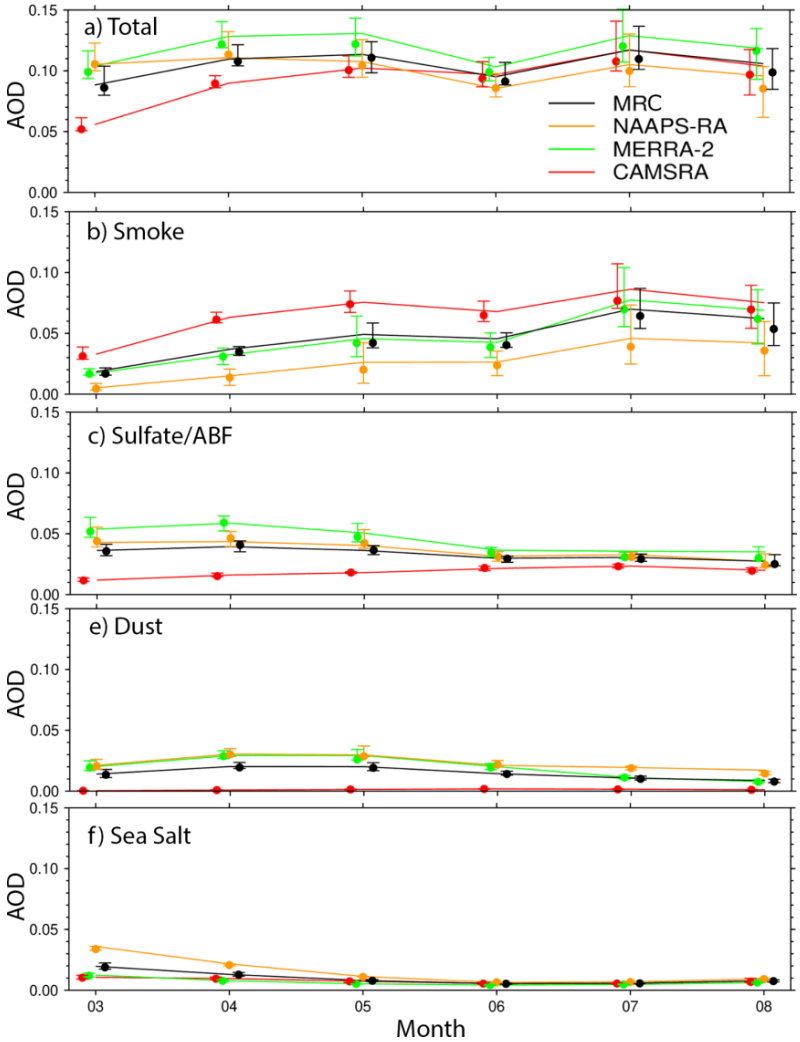

Figure 6. Climatological (2003-2019) seasonal cycle of Arctic (60°-90°N) average total and speciated AODs at 550 nm from the three aerosol reanalyses and the MRC. The top and bottom whiskers represent the 25% and 75% percentiles of monthly AODs, and dots represent the median of monthly AODs.

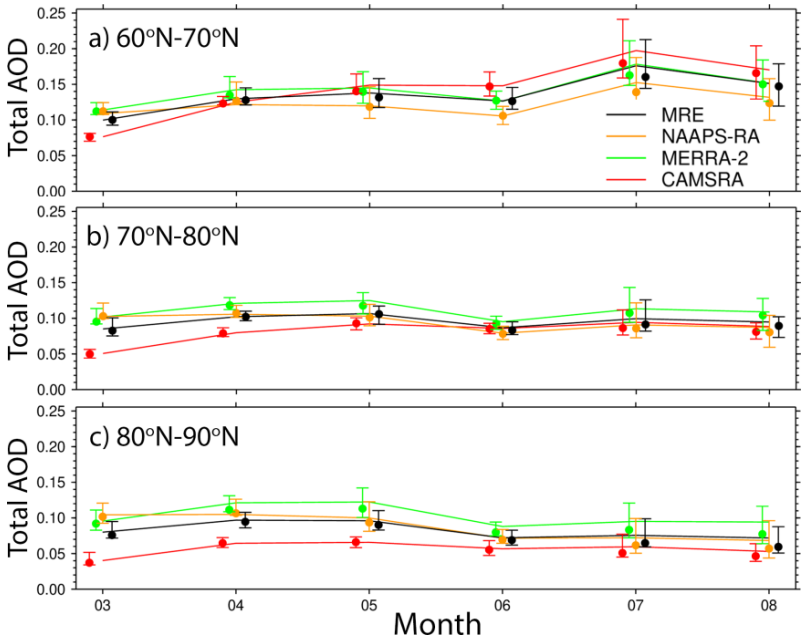

Figure 7. Similar to Figure 6, but for different latitudinal belts and total AOD.

5.2 Interannual variability of AOD in the Arctic

5.2.1 Interannual variability of AOD

There are, as can be seen in ~~Figure~~Fig. 2 (and supported by the MAM/JJA discussion in Sect. 4), significant interannual AOD variabilities, especially for sites close to boreal fire sources. For example, the summertime peak of the total AERONET AOD at Bonanza Creek, Alaska, is around 0.6 - 0.8 in 2004, 2005, and 2019, while it is <~ 0.1-0.2 for other years between 2003-2019. The year to year difference between high- and low-amplitude summertime peak AOD values at Yakutsk, Siberia, can be 6 fold. The MRC shows that these large interannual variabilities consistent with AERONET FM AOD variabilities, are very likely attributable to interannual variabilities in BB smoke.

For sites far from smoke sources, like Ittoqqortoormiit on the east coast of Greenland, Hornsund in Svalbard, and Thule on the northwest coast of Greenland, the high-amplitude peak AODs are about 2-3 times the low-amplitude peak AODs. This interannual spring to summer variability is also largely associated with BB smoke as suggested by the MRC and the coherent variation of the AERONET FM AOD. Some of the strongest AOD events reported in previous studies have been shown to be associated with the long-range transport of BB smoke. For instance, the strong AOD

peak in the summer of 2015 over Hornsund and Andenes was shown to be associated with a series of intense fires that originated in North America (Markowicz et al., 2016). The strong peak AODs in August 2017 over Resolute Bay, Eureka and Thule were most probably related to intense, fire-induced pyroCB events in North America and the long-range transport of high-altitude smoke (Ranjbar et al., 2019; Das et al., 2021). The high amplitude AOD peak in the spring of 2006 over Hornsund was traced to agricultural fires in Eastern Europe (Stohl et al., 2007). The boreal fires in North America in the summer 2004 led to the maximum-amplitude AOD peaks (over the 2003-2019 period of ~~Figure~~Fig. 2) for the two Alaskan sites and enhanced AOD on the pan-Arctic scale (Stohl et al., 2004). Some of the high-amplitude AOD peak events were recorded during intensive field campaigns. These included the ARCTAS/ARCPAC multi-platform campaign in the summer of 2008 (Matsui et al., 2011; Saha et al, 2010; McNaughton et al., 2011) and the NETCARE research vessel (Canadian Arctic) campaign in the spring of 2015 (Abbatt et al., 2019).

The MAN measurements and AERONET sites adjacent to the North Atlantic, the Greenland Sea, and the Norwegian Sea, notably Ittoqqortoormiit, Hornsund, and Andenes have higher CM AODs and higher CM to total AOD ratio compared to other sites: this is due to contributions from sea salt aerosols. Sea salt AOD, indicated by the MRC, is normally higher in MAM than in JJA.

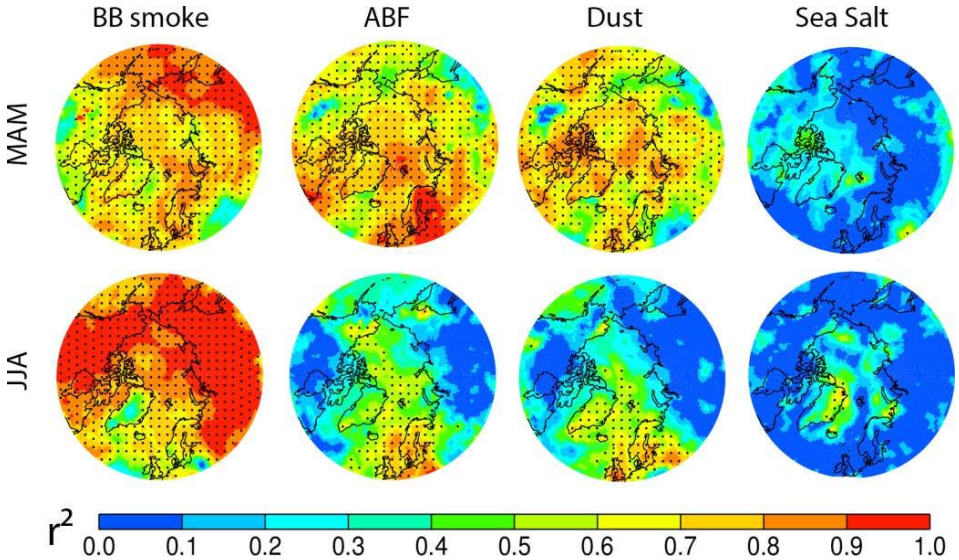

Figure 8. Interannual variability of MRC MAM (upper panel) and JJA-mean (lower panel) total AOD at 550 nm explained by biomass-burning smoke AOD, ABF, dust, and

sea salt aerosols (i.e., the square of the correlation coefficient between speciated AOD and total AOD) respectively. r^2 in dotted area is statistically significant at the 95% level using a two-tailed Student *t* test.

5.2.2 Attribution of AOD interannual variability

It can be observed in ~~Figure~~Fig. 6 that the simulated interannual (60-90°N) AOD variability (represented by the ~~Figure~~Fig. 6 whisker bars) is mostly attributable to the large interannual variability of smoke AOD (especially from May to August). This is consistent across all the reanalysis products. For March and April, the contribution from sulfate/ABF is as important as BB smoke, if not larger. The interannual variation of dust AODs, as indicated with MERRA-2 and NAAPS-RA data, is non-negligible in MAM.

Regarding spatial distribution, ~~Figure~~Fig. 8 shows the interannual variabilities of spring and summer Arctic AOD explained by different aerosol species (i.e~~.~~., the square of the correlation coefficient between speciated AOD and total AOD) suggested by MRC for 2003-2019. Consistent with the variability of monthly AOD time series shown in ~~Figures~~Fig. 2 and 6, both MAM and JJA interannual variabilities are explained mostly by BB smoke, with a higher degree of explanation for JJA than for MAM, and a lower degree of explanation for over the North Atlantic, Norwegian Sea and Greenland than over North American and Eurasian sectors overall. For north of 70°N, smoke explains 60%-80% of MAM and about 80% (except Greenland) of JJA AOD interannual variabilities. Over North American and Eurasian sectors (>60°N), the number is about 100% for JJA. The second-largest contributor is ABF/sulfate and dust for MAM and to a lesser extent for JJA. Contribution from sea salt is the least and is only statistically significant east of Greenland in JJA.

The contribution from ABF/sulfate is above 80% over the industry- and -population-concentrated European and northeast North American sectors and their outflow regions of the North Atlantic, Greenland Sea, Norwegian Sea, and the Arctic Ocean in MAM, while this number decreases to above 60% over Europe and the European Arctic (including water) and is insignificant over North America in JJA. Dust, possibly from Asian and high-latitude sources, could explain some of the interannual AOD variabilities over some regions, e.g~~.~~., Greenland and Greenland Sea in JJA and additionally North Pacific and the Arctic ocean in MAM, however there exist large uncertainties in this evaluation based on the worse verification score of CM compared to FM AOD (Tables 2,3,4). And only CAMSRA among the three reanalyses considers high-latitude dust. Co-variability of species, e.g., BB smoke, ABF/sulfate, and dust, is discernible due to the same transport pathways from the ~~midlatitudes~~mid-latitudes to the Arctic. It is also possible that these species covary because of artifacts introduced by intrinsic treatment in AOD data assimilation for low AOD situations (Zhang et al., 2008).

5.3 Total and speciated AOD trends over 2003-2019

The total AOD ~~trend~~trends for spring and summer over 2003-2019 derived from MODIS, MISR, and for 2006-2019 from CALIOP are presented in ~~Figure~~Fig. 9. Because of the scarcity of valid retrievals over the Arctic, the valid trend analysis is mostly limited to south of 70°N, and the north Atlantic region, and with less coverage in MAM than in JJA from MODIS and MISR and less coverage in JJA than MAM from CALIOP for reasons mentioned in Sect. 5.1.1.

5.3.1 AOD trends for springtime

For MAM, there is a general negative trend in total AOD over the 50-60°N belt and the North Atlantic, with the largest negative trend of -0.06 to -0.10 AOD/decade being over Europe, most probably due to a decrease in ABF/sulfate from decreased anthropogenic emissions as indicated by the reanalyses (~~Figure~~Fig. 10). The negative trend from CALIOP is slightly smaller than those from MODIS and MISR, again possibly attributed to a shorter length of the data record, where earlier and more polluted years for Europe and North America (2003-2006) is not included. All the reanalyses also show a negative trend in total AOD pan-Arctic (-0.01 to -0.02 AOD/decade), except for a close-to-neutral trend over the Arctic ocean and a very slight positive trend over boreal North America from CAMSRA. All the reanalyses suggest that the negative trend over the southeast Siberia and East Asian outflow region is associated with a decrease in BB smoke, and a decrease in ABF/sulfate from NAAPS-RA and MERRA-2 in tandem. Other consistent features found across the reanalyses include the negative trend over Europe associated with decreasing ABF/sulfate, which is possibly related to anthropogenic emission decrease over the past two decades (Breider et al., 2017), as well as a weak positive trend of sea salt over the North Atlantic, which is possibly due to the observed increase in cyclonic activities there (Rinke et al., 2017; Waseda et al., 2021; Valkonen et al., 2021). It is worth noting that NAAPS-RA does not include emission trend for ABF, and MERRA-2 doesn't either after 2008, which means the ABF/sulfate trends seen from these two reanalyses are mostly driven by a negative AOD correction applied by the data assimilation systems. This corroborates the negative trend in ABF/sulfate.

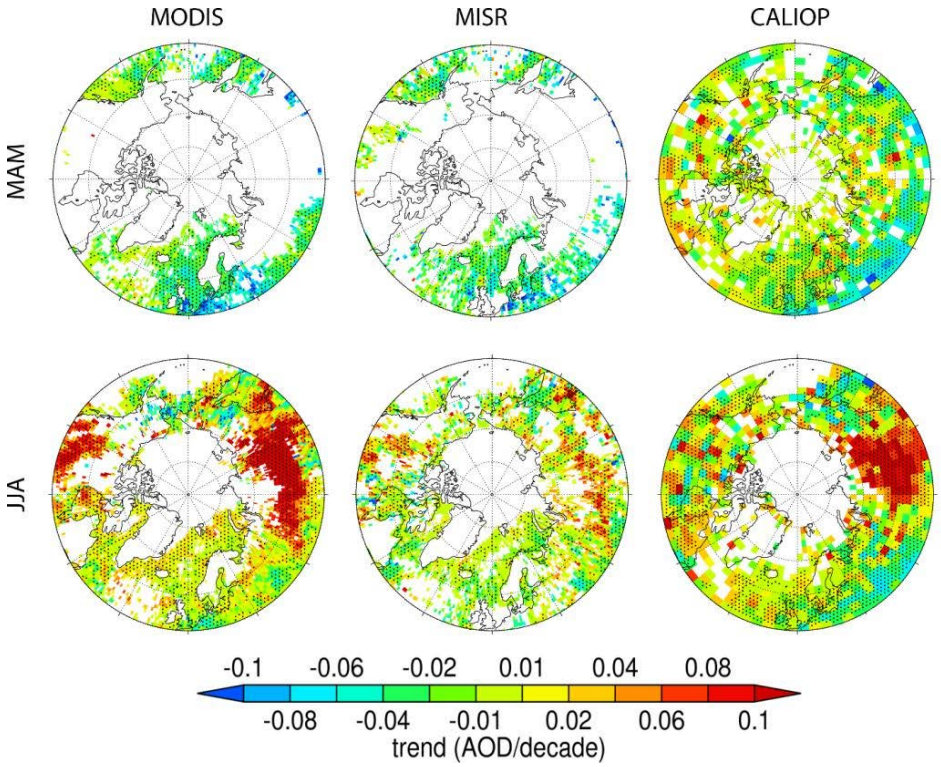

Figure 9. MAM and JJA AOD trends from MODIS, MISR, and CALIOP for the corresponding time periods and AOD wavelengths shown in Figure 3. The trend in the dotted area is statistically significant.

5.3.2 AOD trends for summertime

For JJA, the most prominent feature across all three space-borne sensors is the strong positive trend of total AOD over vast regions of Siberia and North America with a magnitude of around or greater than 0.10 AOD/decade. All the reanalyses capture this positive trend and indicate it is attributed to a significant increase in BB smoke AOD in these regions over 2003-2019 (~~Figure~~Fig. 11). This is in accordance with strong positive regional trends in BB emissions north of 50°N and north of 60°N derived from FLAMBE, a MODIS-fire hotspot-based emission inventory (~~Figure~~Fig. 12), and from other BB emission inventories, e.g., GFED and GFAS (Fig. 2 in McMarty et al., 2021). At the same time, there are negative trends in total AOD over Alaska, northeast of Russia, and North Pacific from the reanalyses, which is seemingly consistent with the trend in remote sensing AODs (though for some satellite datasets the coverage is spotty in these regions). These trends are driven by BB smoke and smoke emission trends as

suggested by all the reanalyses and FLAMBE. In addition, there is a continued negative trend from MAM to JJA in ABF/sulfate over Europe, which is also reflected in total AOD trend, as shown in the reanalyses. This is consistent with the discernible negative though weak trend from the three sensors. JJA AOD trends in dust and sea salt are neutral from the reanalyses.

Besides rising surface temperature, climate phenomena such as the El Niño–Southern Oscillation (ENSO), Arctic Oscillation (AO), and Pacific Decadal Oscillation (PDO) have been reported as affecting fire activity in several key boreal fire source regions (Balzter et al., 2007; Macias Fauria and Johnson, 2007; Kim et al., 2020). However rising surface temperature, probably contributes more to the observed trend in BB emission in the high latitudes. With the rising surface temperature, lightning activity and lightning-caused wildfires in summertime high latitude regions were observed to increase in the past two decades (Zhang et al., 2021; Bieniek et al, 2020; Coogan et al., 2020). In addition, agricultural fire activity in Eastern Europe and European Russia (peaking at April to May) and central Asia and Asiatic Russian (peaking in August) (Korontzi et al, 2006; Hall et al., 2016) also affects the seasonality of total BB emissions. The MAM negative trend in BB smoke may be relevant to a strengthening of agriculture burning regulations in the later part of the 2003-2019 time period. For example, the MAM BB emission maxima in 2003, 2006 and 2008 are all associated with wide-spread springtime agriculture burnings in high latitudes (Korontzi et al, 2006; Stohl et al., 2007; Saha et al., 2010). The aforementioned climate oscillations also modulate interannual variations of the transport of pollutants from the mid latitudes to the Arctic (e.g., Eckhardt et al., 2003; Fisher et al., 2010).

5.3.3 High Arctic AOD trends

For the high Arctic (>70°N), AOD trends are hardly seen with the same color scale as those for the lower latitudes because of lower AOD. Thus, they are shown separately in ~~Figure~~Fig. 13, where time series of MAM and JJA area-mean total, smoke, and ABF/sulfate AODs are shown individually and for all the reanalyses and the MRC over the 2003-2019 time period. There is a negative trend across models in MAM total AOD with -0.017 AOD/decade (-18%/decade), and a positive trend in JJA total AOD with 0.007 AOD/decade (8%decade) based on the MRC. The largest contributor to the MAM negative trend is ABF/sulfate, and the smoke AOD trend is also negative. In the summertime, ABF/sulfate trend continues to be negative; however, the smoke AOD trend turns positive, with a high positive trend of 0.010 AOD/decade (22%/decade). BC AOD trends from MERRA-2 and CAMSRA are dominantly driven by smoke AOD, and have similar trends with smoke AOD in percentage per decade. The negative trend in ABF/sulfate AOD is in line with the decreasing trend in surface sulfate mass concentrations measured over Arctic observational sites (e.g., Breider et al., 2017). The

negative trend in MAM and positive trend in JJA for smoke AOD are consistent with the seasonal-and-area-mean BB emission trends shown in ~~Figure~~Fig. 12 (e,f). The magnitudes of the trends among the three aerosol reanalyses are different, but the signs are the same, corroborating the trend analysis results based on the MRC. These results are consistent with the trend analysis for lower latitude source regions as shown in ~~Figures~~Fig. 9-11. All these results also demonstrate that the Arctic aerosol baseline is changing quickly (Schmale et al., 2021), and the estimation here could contribute to the understanding and quantification of this new baseline.

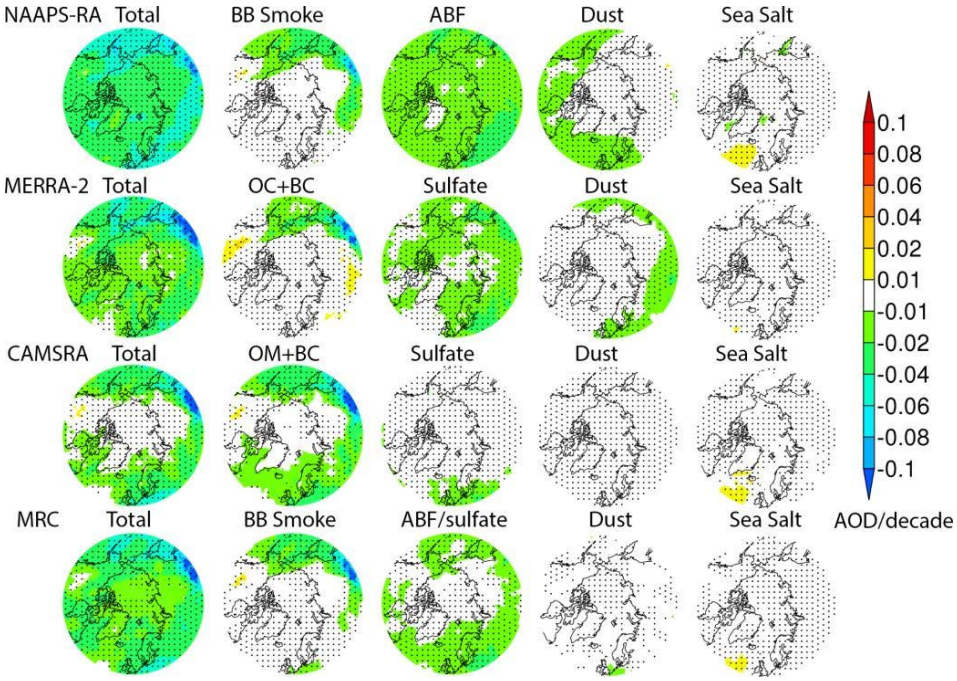

Figure 10. Trends of MAM 550 nm total AOD and contributions from biomass-burning smoke /(BC+OC)/(BC+OM), ABF/Sulfate, dust and sea salt from NAAPS-RA, MERRA-2 and CAMSRA and the MRC.

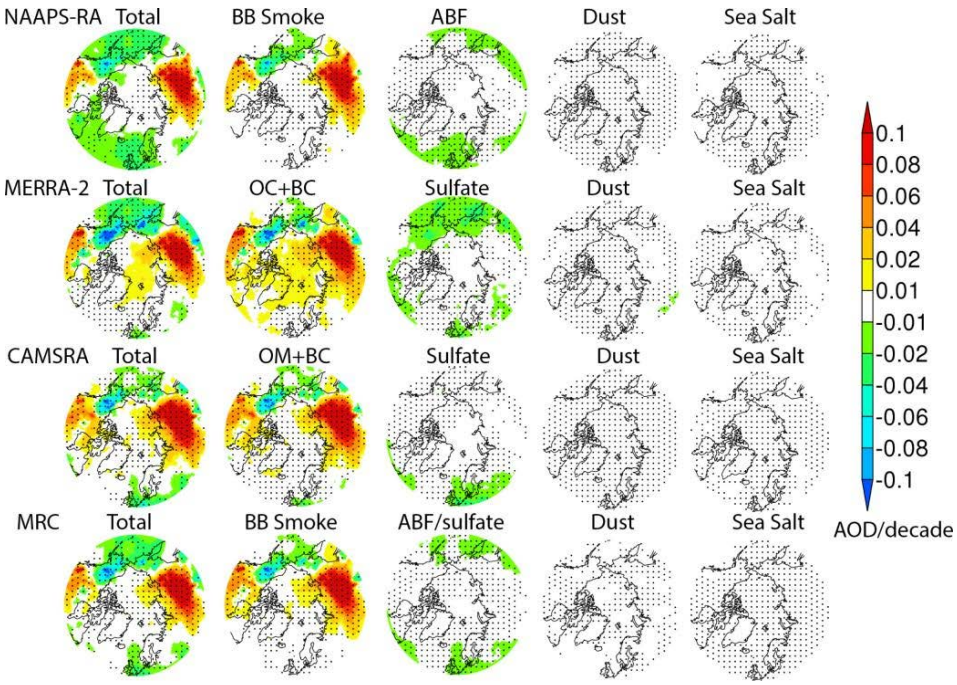

Figure 11. Same as Fig. 10, except for JJA.

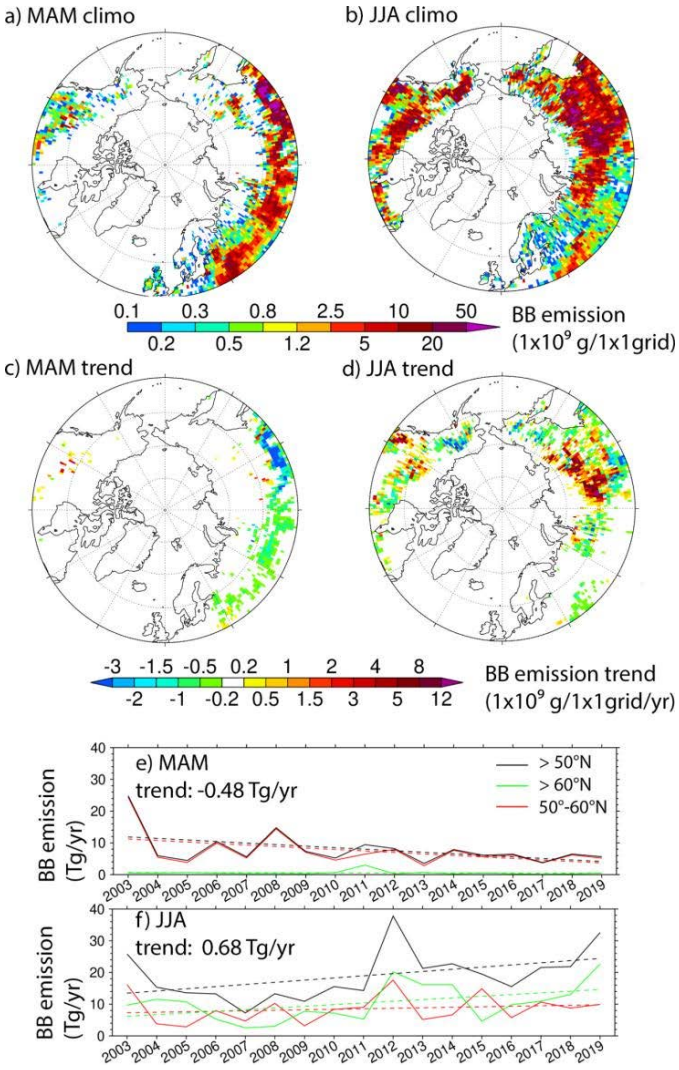

Figure 12. MAM/JJA seasonal total BB smoke particle emission climatology and trend for 2003-2019 derived from FLAMBE (a-d). e) and f) Time series of seasonal-total and area-mean (>50°N, >60°N and 50-60°N) BB smoke (PM2.5 particle) emissions for MAM and JJA respectively. Dashed lines represent linear trends, which are statistically significant with a confidence level of 95%. The trend for north of 50°N is also displayed in texts.

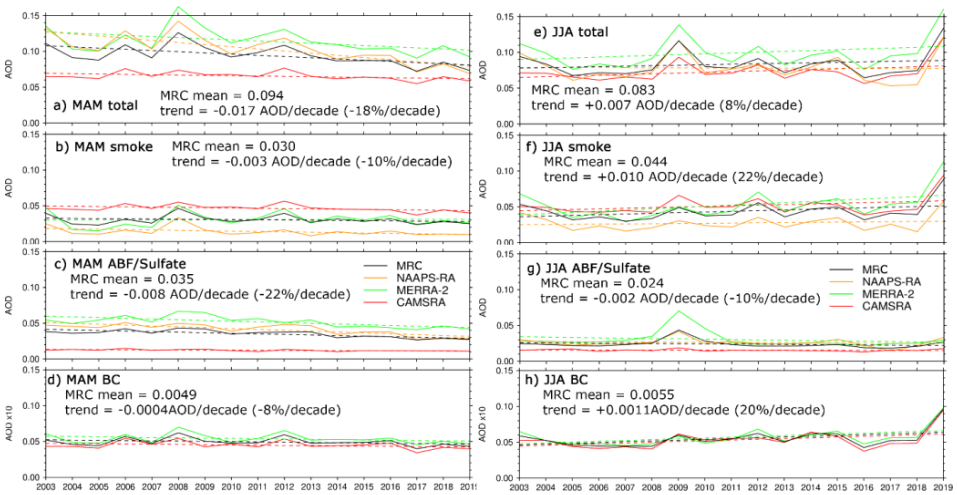

Figure 13. Time series of MAM and JJA 70°-90°N area mean total, BB smoke, ABF/sulfate and BC AODs from the reanalyses and the MRC for 2003-2019 time period. Solid lines are AODs, and dashed lines are linear regressions indicating trends. For easier visualization, BC AOD is multiplied by 10.

Formatted: Font: Bold

~~5.4. Extreme AOD events in the Arctic~~

~~The interannual AOD variability in the Arctic is, as discussed in the previous section, substantial and mostly driven by FM aerosol events (especially biomass burning transport events). We employed resampled, 6hrly AERONET AODs as well as speciated daily/6hrly NAAPS-RA AOD to better demonstrate the frequency and magnitude of the large FM AOD events. We chose NAAPS-RA reanalysis given its slightly better (monthly-mean) FM and total AOD bias, RMSE, and r^2 scores referenced to AERONET data over the Arctic as well as its source-orientated capability of separating BB smoke from other aerosol species.~~

~~5.4.1 General statistics of extreme events~~

~~Figure 14 shows the site by site, total and FM AOD ranges from the 6-hrly AERONET data for all 550 nm retrievals between 2003-2019 (mostly confined to the April-August time frame). Also shown are 6-hrly, pairwise NAAPS-RA AODs that enable model skill evaluation at daily to synoptic scales (see the caption of Figure 14 for the definition of "pairwise" details and note that scatter plots of NAAPS-RA vs AERONET total, FM and CM AOD are shown in Fig. S1). NAAPS-RA verification comparisons relative to MAN data (north of 70°N) is also available as Fig. S2 and S3). NAAPS-RA arithmetic~~

averages are less skillful at predicting CM AODs than FM AODs, and less skillful, on average, for the Arctic region relative to the globe (c.f. Fig. 7 in Lynch et al., 2016). In general, NAAPS-RA largely captures AERONET FM and total AOD ranges: this includes the 5%-95% percentiles of total AERONET AOD, for example (~ 0.02 to ~ 0.20 for most sites), and the larger 0.02 to ~ 0.4-0.6 range of sites with known strong BB smoke influence, (notably Bonanza Creek, Tiksi, and Yakutsk). Mean and median AODs are also comparable to AERONET values. The r^2 values are likewise reasonable (mostly between 0.5-0.7, except for Hornsund, Ittoqqortoormiit, and Kangerlussuaq). The FM AOD r^2 values generally exceed those of the total AOD (> 0.5 for 9 sites and > 0.6 for 7 sites). The maximum AERONT FM AODs for these sites vary between ~ 0.4 (Andenes) to < 2.0 for most sites and > 2.0 for sites with strong BB smoke influence. The maximum NAAPS-RA AOD values are often biased low: this is a common challenge for global aerosol models (e.g. Sessions et al., 2015; Xian et al., 2019). RMSE values for total and FM AOD are generally large (~ AERONET means for the sites suffering from strong smoke influence) and moderately significantly smaller for other sites.

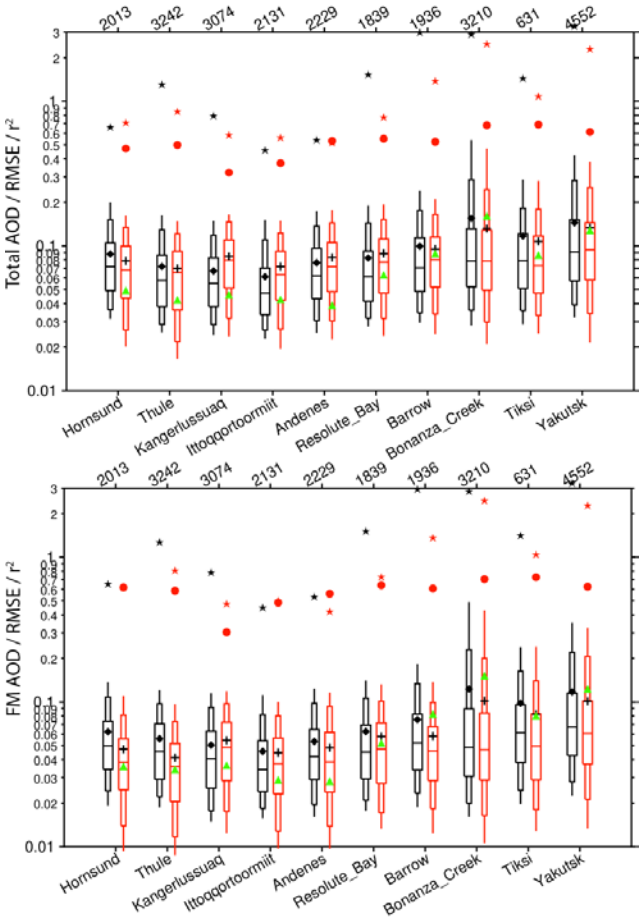

~~Figure 14.~~ ~~Comparison of the 6-hrly (550 nm) total (top) and FM AOD (bottom) of the NAAPS-RA (red) at 95, 90, 75, 50, 25, 10, and 5% percentiles (respective, sequential features of the doubled spear-like symbols from the top tip to the bottom tip) with pairwise AERONET V3L2 data (black) for the ten AERONET sites of Table 1 and Figure 1 for the 2003-2019 time period ("pairwise" refers to those NAAPS-RA AODs that correspond to a resampled AERONET AOD whose ± 3hr bin contains at least one AERONET retrieval). Also shown are the site means of the NAAPS-RA and AERONET AODs ("+" and "♦" symbols respectively) and the NAAPS-RA RMSE ("▲"), the coefficient of determination (r^2) between the NAAPS-RA and AERONET ("●") and the maximum AERONET and NAAPS-RA AODs ("★" and "★" respectively). Note that values greater than 2.0 are not shown. The numbers of 6-hrly AERONET data points for each site are shown just above the plot.~~

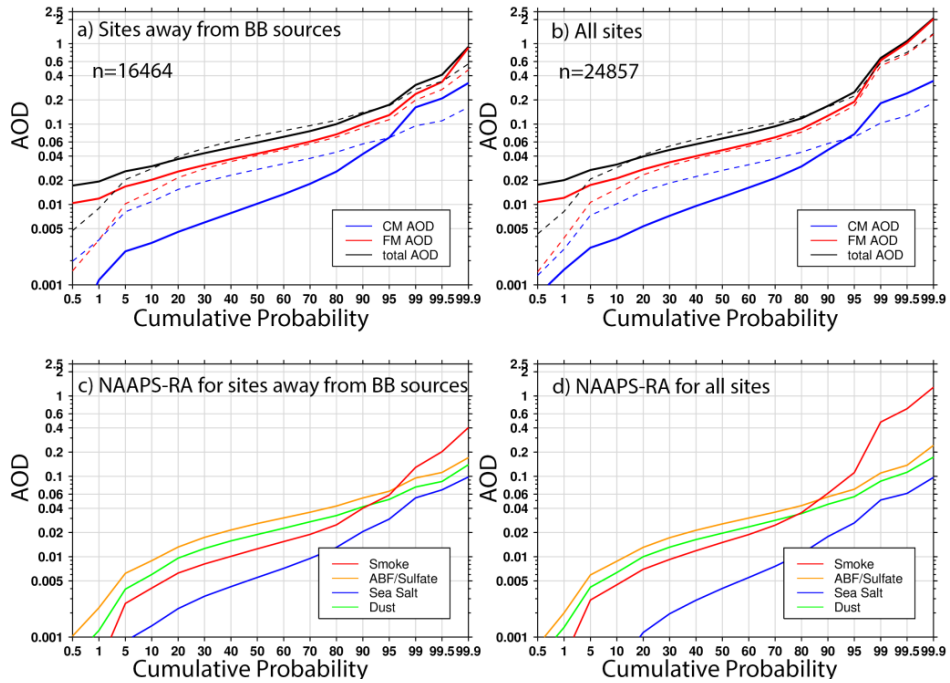

~~**Figure 15.** Upper panes (a, b): cumulative probability distributions of 6-hrly total, FM and CM AOD at 550 nm for AERONET V3L2 data (solid lines) and pair-wise NAAPS-RA (dashed line). Lower panes (c,d): cumulative probability distributions for the corresponding speciated AODs from NAAPS-RA. Left hand panes (a,c): AODs for sites that are distant from BB source regions, including Barrow, Resolute Bay, Kangerlussuaq, Thule, Andenes, Hornsund and Ittoqqootoormiit. Right-hand panes (b,d) all sites north of 60°N. "n" represents the total number of 6-hrly data points over the 2003-2019 period.~~

~~Figure 15 shows the cumulative probability distribution of 6-hrly total, FM and CM AOD at 550 nm for AERONET V3L2 data and pair-wise NAAPS-RA FM and CM AODs (Figures 15a,b) and speciated AODs (Figures 15c,d). For all sites north of 60°N, and for 20%-80% cumulative probability, NAAPS-RA total AOD biases slightly positive (<0.01) due to a relatively large positive bias in CM AOD of ~ 0.01 below a cumulative probability of 95% (a positive bias that is generally evident in Table 2). The bias becomes negative (~ -0.05) above 95%. It is common for models to bias low for extreme events (e.g. Sessions et al. 2015): this negative bias at the largest values of CM AOD~~

could conceivably be associated with an underestimation of the CM AOD generated by sea salt aerosols in the presence of strong winds. We should however, add this caveat: despite the quality-control measures taken to filter out cloud-contaminated AERONET data, the impact of CM residual clouds may still influence estimates of CM AOD.

Table 5. AERONET V2L3 FM, CM and Total AOD at 550nm (with additional filtering for cloud contamination) at different percentiles for the listed Arctic sites. "N" presents total number of 6hrly data during 2003-2019. Also listed are MAN data statistics for data collected north of 70˚N.

	Total | FM | CM AOD at 550nm							
	Median	75%	90%	95%	99%	99.9%	maximum	N
Hornsund	0.072|0.050|0.014	0.105|0.074|0.029	0.151|0.108|0.054	0.200|0.137|0.091	0.386|0.296|0.196	0.580|0.568|0.376	0.663|0.654|0.414	2013
Kangerlussuaq	0.055|0.040|0.009	0.083|0.063|0.020	0.119|0.091|0.038	0.149|0.115|0.060	0.234|0.198|0.111	0.510|0.461|0.221	0.794|0.786|0.244	3074
Resolute_Bay	0.061|0.045|0.011	0.092|0.069|0.021	0.144|0.106|0.041	0.190|0.141|0.063	0.499|0.396|0.160	1.530|1.516|0.452	1.530|1.516|0.452	1839
Barrow	0.071|0.052|0.013	0.114|0.082|0.025	0.176|0.134|0.048	0.241|0.183|0.079	0.466|0.415|0.198	2.999|2.962|0.454	2.999|2.962|0.454	1936
Thule	0.058|0.045|0.007	0.087|0.071|0.015	0.129|0.097|0.036	0.163|0.121|0.061	0.305|0.194|0.179	0.807|0.794|0.315	1.310|1.272|0.328	3242
Ittoqqortoormiit	0.047|0.034|0.006	0.070|0.054|0.015	0.110|0.082|0.033	0.151|0.111|0.058	0.278|0.215|0.161	0.456|0.446|0.329	0.459|0.450|0.342	2131
Andenes	0.062|0.042|0.014	0.096|0.064|0.027	0.137|0.098|0.050	0.174|0.123|0.075	0.277|0.210|0.154	0.451|0.432|0.249	0.541|0.534|0.258	2229
Bonanza_Creek	0.078|0.048|0.022	0.131|0.089|0.036	0.286|0.229|0.059	0.539|0.489|0.086	1.657|1.619|0.246	2.619|2.591|0.499	2.908|2.857|0.541	3210
Yakutsk	0.091|0.067|0.015	0.152|0.115|0.028	0.283|0.220|0.056	0.422|0.353|0.098	0.985|0.968|0.215	3.018|2.972|0.361	3.296|3.259|0.379	4552
Tiksi	0.079|0.061|0.011	0.121|0.096|0.021	0.182|0.163|0.040	0.286|0.239|0.060	0.936|0.915|0.123	1.442|1.413|0.238	1.442|1.413|0.238	631
MAN	0.052|0.029|0.021	0.090|0.062|0.031	0.126|0.097|0.042	0.164|0.118|0.052	0.281|0.253|0.085	0.777|0.761|0.234	0.777|0.761|0.234	520

Above the 95% percentile mark, BB smoke plays a dominant (all sites) Arctic role compared to other aerosol species (Figure 15b,d). Even for sites distant from BB source regions (including Resolute Bay, Kangerlussuaq, Thule, Andenes, Hornsund, Ittoqqootoormiit, and to a mixed extent Barrow as per Eck et al., 2009), BB smoke is the principal driver of AOD variations above the 95% percentile mark (Figure 15a,c). The modal and total AOD values at different percentile levels for the AERONET sites and MAN data collected north of 70°N are provided in Table 5. For the sites closer to BB sources, including Bonanza Creek, Yakutsk and Tiksi, the 99% percentile total AOD and FM AOD are >~ 1.0, while for distant sites the 99% percentile total AOD varies between 0.23-0.50. These extreme smoke cases could be caused by intense fire-induced pyroCB events that inject smoke high in the troposphere or even well into the stratosphere (Fromm et al., 2010; Peterson et al., 2018). An example pyro-CB smoke event that occurred over British Columbia in August 2017 lead to a record-high AOD in the Canadian high Arctic (Ranjbar et al., 2019; Torres et al., 2020). More recently, Eastern Siberian fires burned during June - August 2021 facilitated more than a dozen cases of smoke intrusion into the high Arctic. Some smoke plumes even reached the North Pole and/or its vicinity. For example, on the 5th of August, operational NAAPS (same chemistry and physics, and same BB emission source with NAAPS-RA. NAAPS-RA is not available at the time of this analysis) analyzed a plume of smoke AOD value of 2-3 north of 80°N (Fig. 16). Smoke AOD over the source region was also 2 to >3 with a similar amplitude to the measured at Yakutsk. CALIOP data suggests smoke layer height varying between 1 to 6 km at the source region (vertical distribution of these smoke events is the topic for another manuscript).

For extreme BB smoke events, large particles like ash and soil components emitted from vigorous burning (Schlosser et al., 2017; Reid et al., 2005) can likely be detected to some degree as AERONET CM AOD (see, for example, the correlation between the FM and "weak" CM particle size distributions for Bonanza Creek in Figure 9a of Eck et al., 2009). For extreme AODs that are likely dominated by smoke (above the 99% percentiles of 1.657 at Bonanza Creek, 0.985 at Yakutsk and 0.936 at Tiksi in Table 5 for example), the associated mean CM AOD values were respectively 0.048, 0.031 and 0.033. The larger CM AOD amplitudes (relative to, for example, the JJA means of Table 1) and the rough correlation suggests the presence of detectable CM smoke.

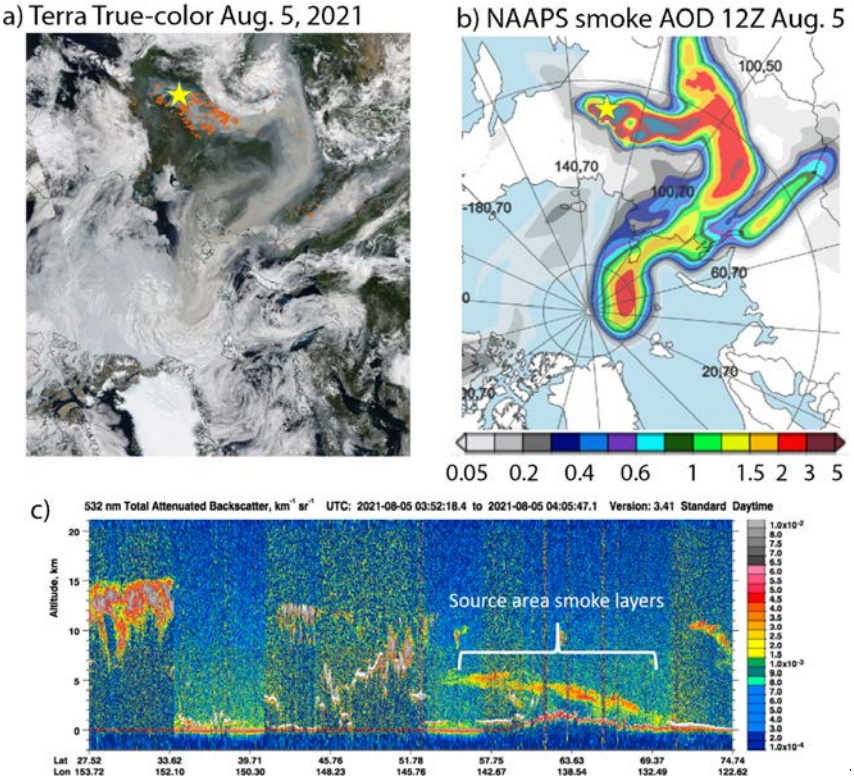

Figure 16. An example of BB smoke intrusion into the high Arctic from fires originated in East Siberia. a) True-color Terra satellite imagery composited on August 5, 2021. 12 September 2012. Red dots represent satellite detected fire hotspots. b) Operational NAAPS smoke AOD analysis valid at 12Z August 5, 2021. c) CALIOP 532 nm attenuated backscatter showing the smoke layers around the source area. The yellow star on a) and b) represents the location of Yakutsk, which experienced a daily mean

total AOD (500nm) of 2.0 (FM AOD ~1.9) and an intra-day peak around 2.5 based on AERONET V3L1.5 data. Satellite imagery courtesy of the MODIS flying on NASA's Terra satellite and CALIOP flying on CALIPSO satellite and available from https://worldview.earthdata.nasa.gov/ and https://www-calipso.larc.nasa.gov/.

Figure 17 shows the geographical distributions of NAAPS-RA total AOD at different percentile levels for March-August 2003-2019. The median ("50 percentile") Arctic AODs (<~ 0.1 and specifically ~0.07 for the AERONET sites from Figure 15) are an order of magnitude smaller than the max AODs. At the 95% percentile mark, clear BB smoke features about the North American and Asian boreal burning regions start to emerge. The maximum AODs are high (greater than 2.0) about those BB source regions and relatively low over the Arctic Ocean (~ 0.3 - 1.0) and the north Atlantic (with the lowest values over Greenland). The maximum AOD generally occurs in July and August: this is associated with peak burning activities (except for the Norwegian Sea area where the maximum AOD occurred in MAM; this is possibly associated with a combined high AOD level from anthropogenic pollution and marine aerosols).

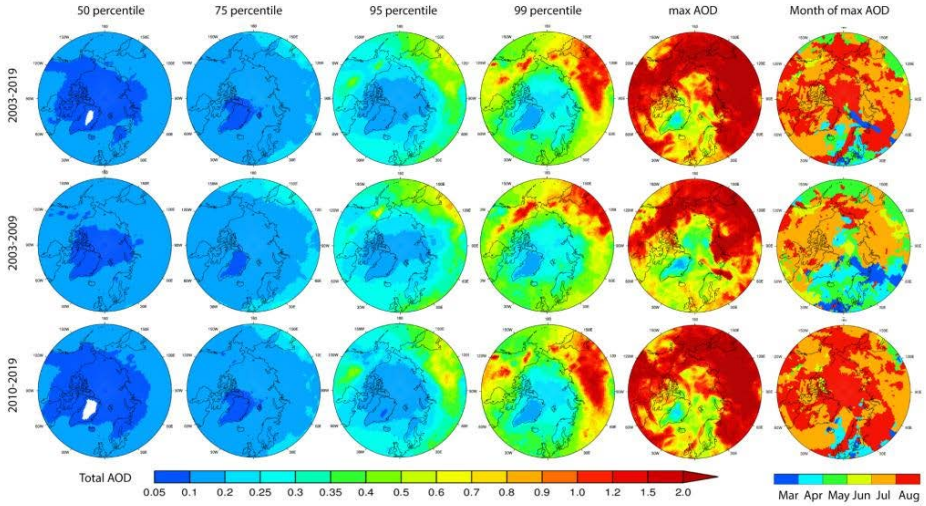

Figure 17. Geographical distributions of NAAPS-RA daily (550 nm) total AOD at different percentile levels for a March-August time frame and (rightmost column) month of the occurrence of maximum AOD for sampling periods of 2003-2019 (upper row), 2003-2009 (middle row), and 2010-2019 (bottom row).

5.4.2 Seasonality and trend of extreme events

Figure 18 presents the seasonal cycle of total and speciated AOD ranges from the NAAPS-RA based on daily and area-averaged (north of 70°N, to stay away from BB source regions) data. The seasonal cycle of monthly mean total AOD looks similar to that in Figure 7b for 70°N-80°N latitudinal mean with relatively higher total AOD in MAM, and lower AOD in JJA and a minimum in June. The spread (bars and whiskers in the plot) of ABF/sulfate AOD values is quite stable through the seasons, with a relatively higher mean/median in MAM than JJA. Sea salt AOD and AOD spread is relatively high in earlier months (March and April) compared to later months. Dust AOD and spread are generally stable through the season, with a visibly higher mean/median in April and May. Smoke AOD and spread exhibit the most prominent seasonal variations among all species, with the lowest mean and spread in March, and increased mean and spread in April, and much higher mean and spread in later months. July and August appear to have the highest mean and spread, and the largest maximum smoke AOD, consistent with Figure 17. These smoke features significantly contribute to the seasonality of extremes in total AOD. It is also noted that for MAM, the means approximately equal the medians, but the means are greater than the medians for JJA and especially so for August. This is because there are more extremes in smoke AOD in the later season, which influences the means.

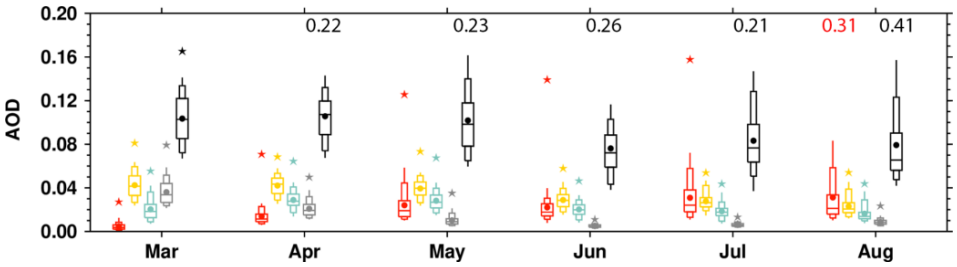

Figure 18. Box and whisker plot of daily and area-averaged (70°N-90°N) speciated AOD at 550 nm from NAAPS-RA (2003-2019) for different months. Each box and whisker column shows AOD at 95, 90, 75, 50, 25, 10, and 5% percentiles. Smoke, ABF/Sulfate, dust, sea salt, and total AODs are presented in red, orange, green, grey, and black colors respectively. Also shown are mean AODs in dots, and maximum AODs in stars. For maximum AOD greater than 0.2 (beyond plotting area), AOD values are shown in number and corresponding colors on the top.

As shown in Sect. 5.3 there is a slightly decreasing trend in MAM and an increasing trend in JJA total AOD in the Arctic during 2003-2019. It is intriguing to explore the possible trend in extreme events. We separate the whole time period into an early (2003-2009) and a late (2010-2019) period (Figure 17, Table 6). 2009 is chosen as the

separation year given the drop in ABF/sulfate emissions due to clean air acts across the U.S. (https://www.epa.gov/air-trends/sulfur-dioxide-trends), Europe and China and the decrease in ABF/sulfate AOD in these regions (Lynch et al., 2016; Zhang et al., 2017) and in the Arctic as shown in Figure 13. Consistent with the BB emission trends in JJA (JJA trend dominates MAM trend as JJA has much higher BB emissions), total AOD at 95% percentile in general increased over the boreal continents, except Alaska and northeastern Siberia in 2010-2019 compared to 2003-2009.

Table 6. Occurrence statistics of high Arctic area-mean (>70˚N) daily BB smoke AOD extreme event (defined as days with smoke AOD above 95% percentile, which is ~0.06) based on 2003-2019 NAAPS-RA. Years without extreme smoke event is omitted.

	Extreme BB smoke days						Mean extreme
	APR	MAY	JUN	JUL	AUG	Annual total	smoke AOD
2003	9	16	0	0	0	25	0.096
2004	0	0	0	12	0	12	0.079
2006	0	0	0	4	0	4	0.121
2008	4	11	0	0	0	15	0.070
2009	0	0	0	0	5	5	0.064
2003-2009 ave	1.9	3.9	0.0	2.3	0.7	8.7	0.086
2010	0	0	1	0	2	3	0.074
2012	0	0	0	3	0	3	0.072
2014	0	0	0	1	2	3	0.065
2015	0	0	2	17	0	19	0.079
2016	0	4	0	0	0	4	0.072
2017	0	0	0	0	13	13	0.098
2019	0	0	0	7	25	32	0.117
2010-2019 ave	0	0.4	0.3	2.8	4.2	7.7	0.083

From the early period to the late period, the high Arctic (>70°N) 50%, 75%, 95% percentile AODs change little, or even slightly decrease, due to decrease in ABF/sulfate, however the maximum AOD value increased in the latter time compared to the early time, indicating stronger extreme BB smoke influence in more recent years. It is also noted that the maximum AOD occurred later in the season (mostly August) in 2010-2019 compared to occurring in March through August in 2003-2009 for the high Arctic (Figure 17). This is likely attributed to the overall lower level of ABF/sulfate, especially in MAM, a shift in extreme smoke events to later season (Table 6) and agriculture burning control for early season (Sect. 5.3.2). The statistics of occurrence of extreme pan-Arctic smoke events (defined as days with 70-90°N area-average daily smoke AOD above 95% percentile) demonstrate a clear shift from all season (both Spring and Summer) to late season, specifically July and August (Table 6). This is consistent with the temporal shift of fire activity to a later time in Siberia over 2003-2018 (Liu et al., 2020), and the projection of emerging pan-Arctic fire regime be marked by

~~shifts in the likelihood of extreme fires later in the growing season (McCarty et al., 2021). An earlier fire season in the boreal region normally suggests a better-managed forecast with fewer large and destructive fires, while a later fire season would indicate the opposite.~~

6. Discussion

The quality control processes applied on the AOD retrievals from MODIS, MISR, and CALIOP help to generate a consistent AOD climatology and trend near the Arctic. The cloud-clearing process on the MISR data and QA processes on the MODIS data removed a good volume of data (about 40% for MISR and MODIS). However, these QA processes help to retain only the best-quality data, which yield a closer magnitude of AOD for MODIS and MISR to AERONET AODs near the 70°N latitude circle (around or less than 0.1), compared to ~0.2 using regular level 3 MODIS and MISR data in ~~figures~~Figs 20 and 23 of Tomasi et al., 2015, especially for springtime. The manual QA process on the AERONET AOD data also reveals more frequent cloud contamination in springtime than in summertime. ~~The regular CALIOP AOD L3 product, with the filled values for low AODs, yielded different spatial and seasonal patterns of AOD (not shown). After removing the pixels with filled~~ Often artificial AOD value of zero are observed over the Arctic in CALIOP V4.2 L2 and L3 data, resulted partially from algorithmically setting altitude bins with retrieval filled values in the aerosol profile to zero, as these represent undetectable levels of faint aerosol (i.e.,Toth et al., 2016; 2018). With AOD=0 values retained in the CALIOP V4.2 L2 data analysis (same processing in CALIOP V4.2 L3), the climatological seasonal mean AOD magnitude is much smaller (about half) than that shown in Fig. 3 and the AOD trends are slightly smaller than those in Fig. 9, although the spatial patterns of the seasonal AOD and trends are similar to those obtained with AOD data after removing the AOD=0 values (Fig. S2). After removing the pixels with filled and zero values, CALIOP AOD seasonal spatial AOD distributions are similar to those from MODIS and MISR.

The total AOD at 550 nm from the three aerosol reanalyses are much more convergent in spatial distribution, magnitude, and seasonality in the Arctic compared to the climate models ~~(e.g., and are similar to those from the remote sensors near the Arctic. For example, for~~ AEROCOM models in Sand et al., 2017, ~~where~~ MAM AODs averaged over nine Arctic AERONET sites (all included in this study) are an order of magnitude different for the highest and lowest AOD models, and peak AOD season varies among winter, spring and summer; In the CMIP5 models in Glantz et al., 2014, ~~where~~ spring and summertime AODs over the Svalbard area also show an order of magnitude difference and there are different seasonality for some of the models~~), and are similar to those from the remote sensors near the Arctic.~~ The possible reasons for ~~this~~the convergence of AOD in the reanalyses include 1) the hourly/daily resolved satellite-

Formatted: Indent: First line: 0"

hotspot-based BB emissions used by these reanalyses apply fine-temporal and interannual-variability-resolved emission constraints; 2) despite that the commonly assimilated satellite AOD (e.g~~.~~., MODIS AOD in all three reanalyses) has limited coverage in the Arctic due to retrieval challenges of dealing with bright surfaces and high cloud coverage, the observational constraint of model fields through assimilation of AOD in the lower latitudes is effective in constraining Arctic AOD to a good extent through transport; 3) more accurate meteorology representations. It is reasonable that the AOD spread among the three reanalyses increases with latitude, and into the early months (e.g., March) when retrieval coverage for lower latitudes is less than summer months.

Except for the chemical processes relevant to conversion of SO_2 to sulfate, the aerosol reanalysis products (or their underlying aerosol models) don't include other new particle formation processes that may be important over the Arctic open water/leads in Springtime or over packed ice during transitional summer to Autumn season (Abbatt et al., 2019; Baccarini et al., 2021). High latitude dust sources, e.g~~.~~., glacier dust, which are present for some areas in the Arctic (Bullard et al., 2016), are only included in CAMSRA, despite that Arctic dust AOD in CAMSRA is much lower than those in the other two models (Fig. 6e).

To show the contribution of biomass burning on total AOD in the Arctic, we approximated BB smoke with the sum of BC and OC/OA from MERRA-2 and CAMSRA. This approximation is rather arguable. It is better suited for JJA than MAM, as the climatological seasonal mean of Arctic AOD is dominated by BB smoke in JJA, which means that BC and OC/OC are mostly from BB sources, while the contribution of BC and OC/OA from anthropogenic sources is relatively higher in early spring (~~Figure 2,3~~Figs. 4, 5). So smoke AOD is overestimated from MERRA-2 and CAMSRA and more so for MAM. This explains the ~~large r~~larger difference in smoke AOD (ratio to total AOD) in MAM than in JJA between the two reanalyses and NAAPS-RA, which explicitly tracks aerosol mass from BB sources (~~Figures~~Figs. 4, 5, 6). While NAAPS-RA includes BC and OA from anthropogenic sources and sulfate into ABF, which is an arguably reasonable configuration for pollution species, as observational studies show a strong correlation between sulfate and elemental BC surface concentrations at pan-Arctic sites away from BB sources, indicating the sources contributing to sulfate and BC are similar and that the aerosols are internally mixed and undergo similar removal (Eckhardt et al., 2015). BB smoke is expected to have different vertical distributions from anthropogenic pollution if smoke is emitted above the boundary layer~~, which sometimes (~10%) is the case for North American boreal fires (Val Martin et al., 2010).~~ . Some estimates based on satellite observations near local noon have suggested that the fraction of smoke escaping the boundary layer is only ~10% (Val Martin et al., 2010), but taking account of

the diurnal cycle of fire activity and potential for pyroconvection, the actual fraction of elevated smoke could be much larger (Fromm et al., 2010; Peterson et al., 2015; Peterson et al., 2017).

Stratospheric aerosols from volcanic eruptions can contribute to the total AOD in the Arctic, especially for the four years after the Mount Pinatubo eruption in 1991 (Herber 2002). For our study period (2003-2019), the eruptions of Kasatochi, Redoubt, Sarychev, and Eyjafjallajökull in August 2008, March 2009, July 2009, and March 2010, respectively, would have affected the stratospheric AOD and thus total column AOD. However, these eruptions are at least one order of magnitude smaller than that of Pinatubo. The stratospheric AOD contribution to the Arctic background AOD is estimated to be relatively small at ~0.01 (from ~~Figure~~Fig. 16 of Thomason et al., 2018; non-Pinatubo affected years in ~~Figure~~Fig. 5 of Herber 2002), despite that locally and over a short period the AOD contribution can be large (e.g., O'Neill et al., 2012). All the reanalyses have some sort of SO_2 and sulfate representation from volcanic degassing emissions, but a full representation for explosive volcanic sources is lacking (except that MERRA-2 has time-varying explosive and degassing volcanic SO_2 before December 31, 2010). The volcanic influence on Arctic AOD, if detectable, would be reflected in the ABF/sulfate AOD in the reanalyses, but its contribution would be much smaller than the anthropogenic counterpart for our study period. It is also worth noting that volcanic activities are not the only influence on the stratospheric aerosol budget: pyroCB-injected BB smoke can also contribute to stratospheric AOD, as discussed earlier. Stratospheric BB smoke was also detected over the Arctic with lidar measurements during the MOSAiC campaign (Engelmann et al., 2021). Stratospheric injection of BB smoke associated with pyroCB events are not represented in the reanalyses, despite that BB emission associated with these pyroCB events are included in the emission inventories with possible large bias in emission amount and height.

Arctic shipping is often brought up as a potentially important source of BC for the Arctic in the future. All of the reanalyses include shipping emissions, although little interannual trend is considered especially for the late period in 2003-2019. However "Arctic shipping is currently only a minor source of black carbon emissions overall" according to the recent Arctic Monitoring and Assessment Programme (AMAP) report (2021).

7. Conclusions

Using remote sensing aerosol optical depth (AOD) retrievals from the Moderate Resolution Imaging Spectroradiometer (MODIS), the Multi-angle Imaging SpectroRadiometer (MISR), and Cloud-Aerosol Lidar with Orthogonal Polarization (CALIOP), and AODs from three aerosol reanalyses, including the U.S. Naval Aerosol

Analysis and Prediction System-ReAnalysis (NAAPS-RA),the NASA Modern-Era Retrospective Analysis for Research and Applications, version 2 (MERRA-2), and the Copernicus Atmosphere Monitoring Service ReAnalysis (CAMSRA), and ground-based Aerosol Robotic Network (AERONET) data, we have reported the Arctic/High-Arctic (defined as 60°-90°N/70°-90°N) AOD climatology, ~~trend~~ and ~~-~~ trend ~~extreme event statistics~~ for spring (March-April-May, MAM) and summer (June-July-August, JJA) seasons during 2003-2019.

1) ***Arctic AOD climatology***: The total AODs from space-borne remote sensing and the aerosol reanalyses show quite consistent climatological spatial patterns and interannual trends for both spring and summer seasons for the lower-Arctic (60-70°N), where remote sensing data is available. AOD trends for the high Arctic from the reanalyses have consistent signs too. Climatologically, fine-mode (FM) AOD dominates coarse-mode (CM) AOD in the Arctic. Based on the reanalyses, biomass burning (BB) smoke AOD increases from March to August associated with seasonality of BB activities in the boreal region (>50°N); Sulfate/Anthropogenic and biogenic fine (ABF) AOD is slightly higher in MAM than in JJA; sea salt AOD is highest in March and decreases with time into later spring and summer; contribution of dust AOD to total AOD is non-negligible in April and May. The latitudinal gradient of AOD is larger in JJA than in MAM, consistent with observed more efficient removal in summertime (Garrett et al., 2011). Among aerosol species, black carbon (BC) is a very efficient light absorber, and climate forcing agent (e.g~~.~~.., Bond et al., 2013). We show that over the Arctic, the contribution of BC AOD from BB source overwhelms anthropogenic sources in both MAM and JJA, and more so in JJA during 2003-2019.

2) ***Interannual AOD trend***: Total AOD exhibits a general negative trend in the Arctic in MAM, and strong positive trends in North ~~America~~Americas, Eurasia boreal regions (except Alaska and northeast Siberia) in JJA. For the high Arctic, the total AOD trend is -0.017/decade (-18%/decade) for MAM and 0.007/decade (8%/decade) for JJA based on the multi-reanalysis-consensus (MRC). The total AOD trends are driven by an overall decrease in sulfate/ABF AOD in both seasons (-0.008/decade, or -22%/decade for MAM and -0.002/decade or -10%/decade for JJA), and a negative trend in MAM (-0.003/decade or -10%/decade) and a strong positive trend in JJA (0.01/decade or 22%/decade) from biomass burning smoke AOD. The decreasing trend in sulfate in the Arctic in recent decades is in line with other studies using surface concentration measurement (e.g., Eckhardt et al., 2015). The smoke AOD trends are

consistent with MODIS fire-hotspot-based BB emission trends over the boreal continents.

3) ***Impact of BB smoke on AOD interannual variability***: The interannual variability of total AOD in the Arctic is substantial and predominantly driven by fine-mode, and specifically BB smoke AOD in both seasons and more so in JJA than in MAM. For AERONET sites close to BB emission sources, the difference in monthly total AOD can be 6-fold for high versus low AOD years. For remote regions away from BB sources, the interannual variability of total AOD can also be explained mostly by smoke AOD.

~~4) ***Extreme AOD events*** during spring and summer in the Arctic, defined as AOD greater than the 95% percentile value, are mainly attributed to BB smoke transport events as expected. The median of 6hrly total AOD for all AERONET sites in the Arctic during 2003-2019 is ~0.07, and the 95% percentile is ~0.22. With the general decreasing trends in MAM and increasing trend in BB emissions, the AOD extreme events have a tendency to occur later in the season, ie. July and August, in the latter decade rather than spreading over March-August in the early decade during 2003-2019. Global warming is expected to continue leading to drier conditions and increased fire activities in the high latitudes (McCarty et al., 2021), making the Arctic more susceptible to extreme smoke events.~~

~~5)~~4) ***Overall performance of the aerosol reanalyses***: The aerosol reanalyses yield much more convergent AOD results than the climate models (e.g~~.~~.. AeroCOM~~,~~ models in Sand et al., 2017; CMIP5 models in Glantz et al., 2014) and verify with AERONET to some good extent, which corroborates the climatology and trend analysis. Speciated AODs appear more diverse than the total AOD among the three reanalyses, and a little more so for MAM than for JJA. NAAPS-RA and MERRA-2 total and FM AODs verify better in the Arctic than CAMSRA, which tends to have a high bias in FM overall. The reanalyses generally perform better in FM than CM. The three reanalyses exhibit different latitudinal AOD gradients, especially in summertime, indicating different removal efficiencies. The emerging capability of assimilating OMI Aerosol Index (AI) to constrain absorptive aerosol amount, could potentially fill in the observational gaps for aerosol data assimilation in reanalyses over the Arctic (Zhang et al., 2021). With more advanced retrieval algorithms on the current space-borne sensors for over snow/ice, new sensors on future satellites, improvements on the underlying meteorology and aerosol representations in models, improvements in aerosol reanalysis are expected.

The results presented here provide a baseline of AOD spatiotemporal distribution, magnitude, and speciation over the Arctic during spring and summer seasons for the recent two decades. This will help improve aerosol model evaluations and better constrain aerosol radiative and potentially indirect forcing calculation to evaluate aerosol impact in the Arctic amplification. For example, the contribution of reduction in sulfate to Arctic surface warming in recent decades (e.g., Shindell and Faluvegi, 2009; Breider et al., 2017) could potentially be better quantified, with the caveat that speciated AOD have larger uncertainties than total AOD in the reanalyses. The AOD statistics could also provide background information for field campaign data analysis and future field campaign planning in a larger climate context. It is also recommended that climate models should take into account BB emissions besides anthropogenic climate forcers and BB interannual variabilities and trends in Arctic climate change studies.

Appendix A. Summary of data used in the study

Products	Data	resolution	time
MODIS (Moderate Resolution Imaging Spectroradiometer) C6.1L3	550nm AOD	1°x1° monthly	2003-2019
MISR (Multi-angle Imaging SpectroRadiometer) V23	558nm AOD	1°x1°, monthly	2003-2019
CALIOP (Cloud-Aerosol Lidar with Orthogonal Polarisation) V4.2L2	532nm AOD	2°x5°, monthly	2006-2019
AERONET (AErosol RObotic NETwork) V2L3	SDA total, FM, CM AOD at 550nm	6hrly, monthly	2003-2019
MAN (Marine Aerosol Network) Level2	SDA total, FM, CM AOD at 550nm	6hrly	2003-2019
MERRA-2 (Modern-Era Retrospective Analysis for Research and Applications, v2)	Total and speciated AOD at 550nm	0.5°lat x0.63°lon, monthly	2003-2019
CAMSRA (Copernicus Atmosphere Monitoring Service Reanalysis)	Total and speciated AOD at 550nm	0.7°x0.7°, monthly	2003-2019
NAAPS-RA v1 (Navy Aerosol Analysis and Prediction System reanalysis v1)	Total and speciated AOD at 550nm	1°x1°, 6hrly, monthly	2003-2019
MRC (Multi-Reanalysis-Consensus)	Total and speciated AOD at 550nm	1°x1°, monthly	2003-2019
FLAMBE (Fire Locating and Modeling of Burning Emissions) v1.0	BB smoke emission flux	1°x1°, monthly	2003-2019

Note: These are final form of data used in the result section. Some pre-processing and quality-control were applied to remote sensing data as described in the data section.

Code and Data Availability: All data supporting the conclusions of this manuscript are available either through the links provided below or upon request.
AERONET Version 3 Level 2 data: http://aeronet.gsfc.nasa.gov
MAN data: https://aeronet.gsfc.nasa.gov/new_web/maritime_aerosol_network.html
MODIS DA-quality AOD: https://nrlgodae1.nrlmry.navy.mil/cgi-bin/datalist.pl?dset=nrl_modis_l3&summary=Go
Or https://modaps.modaps.eosdis.nasa.gov/services/about/products/c61-nrt/MCDAODHD.html
MISR AOD: ftp://l5ftl01.larc.nasa.gov/misrl2l3/MISR/MIL2ASAE.003/
CALIOP from NASA Langley Research Center Atmospheric Science Data Center: https://doi.org/10.5067/CALIOP/CALIPSO/LID_L2_05kmAPro-Standard-V4-20 for the Version 4.2 CALIPSO Level 2 5 km aerosol profile and https://doi.org/10.5067/CALIOP/CALIPSO/LID_L2_05kmALay-Standard-V4-20 for aerosol layer products. Further QAed data are available upon request.

NAAPS RA AOD: https://usgodae.org//cgi-bin/datalist.pl?dset=nrl_naaps_reanalysis&summary=Go
MERRA-2 AOD: https://disc.gsfc.nasa.gov/datasets/M2TMNXAER_V5.12.4/summary?keywords=%22MERRA-2%22
CAMSRA AOD: https://www.ecmwf.int/en/research/climate-reanalysis/cams-reanalysis
FLAMBE BB smoke inventory is available upon request from U.S. NRL.

Author contributions: P.X. and J.Z designed this study. P.X. performed most of the data analysis and wrote the initial manuscript. T.T., B.S. and E.H. helped with processing of CALIOP, MISR and MODIS AOD data respectively. All authors contributed to scientific discussion, writing and revision of the manuscript.

Competing interests: The authors declare that they have no conflict of interest.

Acknowledgments

We thank the NASA AERONET and MAN, and Environment and Climate change Canada AEROCAN groups for the sun-photometer data, and NASA MODIS, MISR and CALIOP teams for the AOD data used in the study. We acknowledge NASA GMAO, ECMWF and U.S. ONR and NRL for making the aerosol reanalysis products available. We acknowledge the use of imagery from the NASA Worldview application (https://worldview.earthdata.nasa.gov, last access: Sept 26 2021), part of the NASA Earth Observing System Data and Information System (EOSDIS).

Financial support

The authors acknowledge supports from NASA's Interdisciplinary Science (IDS) program (grant no. ~~80HQTR20T0066~~80NSSC20K1260), NASA's Modeling, Analysis and Prediction (MAP) program (NNX17AG52G) and the Office of Naval Research Code 322. N.O. and K.R's work is supported by Canadian Space Agency, SACIA-2 project, Ref. No. 21SUASACOA, ESS-DA program.

References

Abbatt, J. P. D., Leaitch, W. R., Aliabadi, A. A., Bertram, A. K., Blanchet, J.-P., Boivin-Rioux, A., et al. (2019). Overview paper: New insights into aerosol and climate in the Arctic. *Atmospheric Chemistry and Physics*, **19**(4), 2527– 2560. https://doi.org/10.5194/acp-19-2527-2019

AboEl-Fetouh, Y., O'Neill, N. T., Ranjbar, K., Hesaraki, S., Abboud, I., & Sobolewski, P. S. (2020). Climatological-scale analysis of intensive and semi-intensive aerosol parameters derived from AERONET retrievals over the Arctic. *Journal of Geophysical Research: Atmospheres*, *125*, e2019JD031569. https://doi.org/10.1029/2019JD031569

Formatted: Font: Bold

Formatted: Space After: 12 pt, Pattern: Clear (White)

Formatted: English (Canada)

AMAP, 2021. Impacts of Short-lived Climate Forcers on Arctic Climate, Air Quality, and Human Health. Summary for Policy-makers. Arctic Monitoring and Assessment Programme (AMAP), Tromsø, Norway. 20 pp

Baccarini, A., Karlsson, L., Dommen, J. *et al.* Frequent new particle formation over the high Arctic pack ice by enhanced iodine emissions. *Nat Commun* **11,** 4924 (2020). https://doi.org/10.1038/s41467-020-18551-0

Balzter, H., F. F. Gerard, C. T. George, C. S. Rowland, T. E. Jupp, I. McCallum, A. Shvidenko, S. Nilsson, A. Sukhinin, A. Onuchin, C. Schmullius, Impact of the Arctic Oscillation pattern on interannual forest fire variability in central Siberia. *Geophys. Res. Lett.* **32**, L14709 (2005).

Baibakov, K., O'Neill, N. T., Ivanescu, L., Duck, T. J., Perro, C., Herber, A., Schulz, K.-H., and Schrems, O.: Synchronous polar winter starphotometry and lidar measurements at a High Arctic station, AMT, 8, 3789-3809, doi:10.5194/amt-8-3789-2015, 2015.

Bieniek, P. A., Bhatt, U. S., York, A., Walsh, J. E., Lader, R., Strader, H., Ziel, R., Jandt, R. R., & Thoman, R. L. (2020). Lightning Variability in Dynamically Downscaled Simulations of Alaska's Present and Future Summer Climate, *Journal of Applied Meteorology and Climatology*, *59*(6), 1139-1152.

Birch, C. E., Brooks, I. M., Tjernström, M., Shupe, M. D., Mauritsen, T., Sedlar, J., Lock, A. P., Earnshaw, P., Persson, P. O. G., Milton, S. F., and Leck, C.: Modelling atmospheric structure, cloud and their response to CCN in the central Arctic: ASCOS case studies, Atmos. Chem. Phys., 12, 3419–3435, https://doi.org/10.5194/acp-12-3419-2012, 2012.

Boisvert, L.N., A.A. Petty and J.C. Stroeve, 2016: The Impact of the Extreme Winter 2015/16 Arctic Cyclone on the Barents–Kara Seas. Monthly Weather Review, **144** (11), 4279–4287, doi:10.1175/mwr-d-16-0234.1.

Bossioli, E., Sotiropoulou, G., Methymaki, G., & Tombrou, M. (2021). Modeling extreme warm-air advection in the Arctic during summer: The effect of mid-latitude pollution inflow on cloud properties. *Journal of Geophysical Research: Atmospheres*, *126*, e2020JD033291. https://doi.org/10.1029/2020JD033291

Breider, T. J., Mickley, L. J., Jacob, D. J., Wang, Q., Fisher, J. A., Chang, R. Y. W., and Alexander, B.: Annual distributions and sources of Arctic aerosol components, aerosol optical depth, and aerosol absorption, J. Geophys. Res.-Atmos., 119, 4107–4124, https://doi.org/10.1002/2013JD020996, 2014.

Breider, T. J., Mickley, L. J., Jacob, D. J., Ge, C., Wang, J., Payer Sulprizio, M., Croft, B., Ridley, D. A., McConnell, J. R., Sharma, S., Husain, L., Dutkiewicz, V. A.,

Eleftheriadis, K., Skov, H., and Hopke, P. K.: Multidecadal trends in aerosol radiative forcing over the Arctic: Contribution of changes in anthropogenic aerosol to Arctic warming since 1980, J. Geophys. Res.-Atmos., 122, 3573–3594, https://doi.org/10.1002/2016JD025321, 2017.

Bullard, J. E., et al. (2016), High-latitude dust in the Earth system, Rev. Geophys., 54, 447– 485, doi:10.1002/2016RG000518

Campbell, J. R., Tackett, J. L., Reid, J. S., Zhang, J., Curtis, C. A., Hyer, E. J., ... & Winker, D. M. (2012). Evaluating nighttime CALIOP 0.532 μm aerosol optical depth and extinction coefficient retrievals. *Atmospheric Measurement Techniques*, *5*(9), 2143-2160.

Colarco, P. R., R. A. Kahn, L. A. Remer, and R. C. Levy, 2014: Impact of satellite viewing-swath width on global and regional aerosol optical thickness statistics and trends. *Atmospheric Measurement Techniques*, **7,** 2313-2335.

Comiso, J. C., Large Decadal Decline of the Arctic Multiyear Ice Cover (2012). J. Climate, Vol., 25. 1176-1193. https://doi.org/10.1175/JCLI-D-11-00113.1

Coogan, S. C. P., Cai, X., Jain, P., and Flannigan, M. D. (2020) Seasonality and trends in human- and lightning-caused wildfires ≥ 2 ha in Canada, 1959–2018. *International Journal of Wildland Fire* **29**, 473-485. https://doi.org/10.1071/WF19129

Coopman, Q., Garrett, T. J., Finch, D. P., & Riedi, J. (2018). High sensitivity of arctic liquid clouds to long-range anthropogenic aerosol transport. Geo-physical Research Letters, 45, 372–381. https://doi.org/10.1002/2017GL075795

Dai, A., Luo, D., Song, M., & Liu, J. (2019). Arctic amplification is caused by sea-ice loss under increasing CO_2. *Nature Communications*, **10**(1), 121. https://doi.org/10.1038/s41467-018-07954-9

Dall´Osto, M., Beddows, D. C. S., Tunved, P., Krejci, R., Ström, J., Hansson, H.-C., et al. (2017). Arctic sea ice melt leads to atmospheric new particle formation. *Scientific Reports*, **7**(1), 3318. https://doi.org/10.1038/s41598-017-03328-1

Dang, C., S. G. Warren, Q. Fu, S. J. Doherty, M. Sturm, and J. Su (2017), Measurements of light-absorbing particles in snow across the Arctic, North America, and China: Effects on surface albedo, J. Geophys. Res. Atmos., 122, 10,149–10,168, doi:10.1002/2017JD027070.

Das, S., Colarco, P. R., Oman, L. D., Taha, G., and Torres, O.: The long-term transport and radiative impacts of the 2017 British Columbia pyrocumulonimbus smoke aerosols in the stratosphere, Atmos. Chem. Phys., 21, 12069–12090, https://doi.org/10.5194/acp-21-12069-2021, 2021.

DeRepentigny, P., Jahn, A., Holland, M., Fasullo, J., Lamarque, J.-F., Hannay, C., Mills, M., Bailey, D., Tilmes, S., and Barrett, A.: Impact of CMIP6 biomass burning emissions on Arctic sea ice loss, EGU General Assembly 2021, online, 19–30 Apr 2021, EGU21-9020, https://doi.org/10.5194/egusphere-egu21-9020, 2021.

Eck, T. F., et al. (2009), Optical properties of boreal region biomass burning aerosols in central Alaska and seasonal variation of aerosol optical depth at an Arctic coastal site, J. Geophys. Res., 114, D11201, doi:10.1029/2008JD010870.

Eckhardt, S., A. Stohl, S. Beirle, N. Spichtinger, P. James, C. Forster, C. Junker, T. Wagner, U. Platt, and S. G. Jennings (2003), The North Atlantic Oscillation controls air pollution transport to the Arctic, Atmos. Chem. Phys., 3(5), 1769–1778, doi:10.5194/acp-3-1769-2003.

Eckhardt, S., Quennehen, B., Olivié, D. J. L., Berntsen, T. K., Cherian, R., Christensen, J. H., Collins, W., Crepinsek, S., Daskalakis, N., Flanner, M., Herber, A., Heyes, C., Hodnebrog, Ø., Huang, L., Kanakidou, M., Klimont, Z., Langner, J., Law, K. S., Lund, M. T., Mahmood, R., Massling, A., Myriokefalitakis, S., Nielsen, I. E., Nøjgaard, J. K., Quaas, J., Quinn, P. K., Raut, J.-C., Rumbold, S. T., Schulz, M., Sharma, S., Skeie, R. B., Skov, H., Uttal, T., von Salzen, K., and Stohl, A.: Current model capabilities for simulating black carbon and sulfate concentrations in the Arctic atmosphere: a multi-model evaluation using a comprehensive measurement data set, Atmos. Chem. Phys., 15, 9413–9433, https://doi.org/10.5194/acp-15-9413-2015, 2015.

Engelmann, R., Ansmann, A., Ohneiser, K., Griesche, H., Radenz, M., Hofer, J., Althausen, D., Dahlke, S., Maturilli, M., Veselovskii, I., Jimenez, C., Wiesen, R., Baars, H., Bühl, J., Gebauer, H., Haarig, M., Seifert, P., Wandinger, U., and Macke, A.: Wildfire smoke, Arctic haze, and aerosol effects on mixed-phase and cirrus clouds over the North Pole region during MOSAiC: an introduction, Atmos. Chem. Phys., 21, 13397–13423, https://doi.org/10.5194/acp-21-13397-2021, 2021.

Evangeliou, N., Balkanski, Y., Hao, W. M., Petkov, A., Silverstein, R. P., Corley, R., Nordgren, B. L., Urbanski, S. P., Eckhardt, S., Stohl, A., Tunved, P., Crepinsek, S., Jefferson, A., Sharma, S., Nøjgaard, J. K., and Skov, H.: Wildfires in northern Eurasia affect the budget of black carbon in the Arctic – a 12-year retrospective synopsis (2002–2013), Atmos. Chem. Phys., 16, 7587–7604, https://doi.org/10.5194/acp-16-7587-2016, 2016.

Fisher, J. A. *et al*. Sources, distribution, and acidity of sulfate-ammonium aerosol in the Arctic in winter-spring. *Atmos Environ* **45**, 7301–7318, https://doi.org/10.1016/j.atmosenv.2011.08.030 (2011).

Fisher, J. A., et al. (2010), Source attribution and interannual variability of Arctic pollution in spring constrained by aircraft (ARCTAS, ARCPAC) and satellite (AIRS)

observations of carbon monoxide, Atmos. Chem. Phys., 10(3), 977–996, doi:10.5194/acp-10-977-2010.

Flanner, M. G., Zender, C. S., Randerson, J. T., & Rasch, P. J. (2007). Present-day climate forcing and response from black carbon in snow. *Journal of Geophysical Research*, *112*(September 2006), D11202. https://doi.org/10.1029/2006JD008003

Flanner, M. G., C. S. Zender, P. G. Hess, N. M. Mahowald, T. H. Painter, V. Ramanathan, and P. J. Rasch (2009), Springtime warming and reduced snow cover from carbonaceous particles, Atmos. Chem. Phys., 9(7), 2481–2497, doi:10.5194/acp-9-2481-2009.

Flannigan, M. D., and J. B. Harrington, 1988: A study of the relation of meteorological variables to monthly provincial area burned by wildfire in Canada (1953-1980). *J. Appl. Meteorol.*, **27,** 441-452.

Fromm, M., Lindsey, D. T., Servranckx, R., Yue, G., Trickl, T., Sica, R., Doucet, P., & Godin-Beekmann, S. (2010). The Untold Story of Pyrocumulonimbus, Bulletin of the American Meteorological Society, 91(9), 1193-1210.

Gabric, A., Matrai, P., Jones, G., & Middleton, J. (2018). The nexus between sea ice and polar emissions of marine biogenic aerosols. *Bulletin of the American Meteorological Society*, **99**(1), 61– 81. https://doi.org/10.1175/BAMS-D-16-0254.1

Garay, M. J., and Coauthors, 2020: Introducing the 4.4 km spatial resolution Multi-Angle Imaging SpectroRadiometer (MISR) aerosol product. *Atmospheric Measurement Techniques*, **13,** 593-628.

Garrett, T. J., Zhao, C., and Novelli, P.: Assessing the relative contributions of transport efficiency and scavenging to seasonal variability in Arctic aerosol, Tellus B, 62, 190–196, https://doi.org/10.1111/j.1600-0889.2010.00453.x, 2010.

Garrett, T. J., Brattström, S., Sharma, S.,Worthy, D. E., and Novelli, P.: The role of scavenging in the seasonal transport of black carbon carbon and sulfate to the Arctic, Geophys. Res. Lett., 38, L16805, https://doi.org/10.1029/2011GL048221, 2011.

Giglio, L., Randerson, J. T., and van der Werf, G. R.: Analysis of daily, monthly, and annual burned area using the fourthgeneration global fire emissions database (GFED4), J. Geophys. Res.-Biogeo., 118, 317–328, https://doi.org/10.1002/jgrg.20042, 2013.

Giles, D. M., Sinyuk, A., Sorokin, M. G., Schafer, J. S., Smirnov, A., Slutsker, I., Eck, T. F., Holben, B. N., Lewis, J. R., Campbell, J. R., Welton, E. J., Korkin, S. V., and Lyapustin, A. I.: Advancements in the Aerosol Robotic Network (AERONET) Version 3 database – automated near-real-time quality control algorithm with improved cloud screening for Sun photometer aerosol optical depth (AOD) measurements, Atmos. Meas. Tech., 12, 169–209, https://doi.org/10.5194/amt-12-169-2019, 2019.

Glantz, P., Bourassa, A., Herber A., Iversen T., Karlsson J., Kirkevag, A., Maturilli, M., Seland, O., Stebel, K., Struthers, H., Tesche, M., and Thomason L., (2014), Remote sensing of aerosols in the Arctic for an evaluation of global climate model simulations, J. Geophys. Res. Atmos., 119, 8169–8188, doi:10.1002/2013JD021279.

Goosse, H., Kay, J.E., Armour, K.C. *et al.* Quantifying climate feedbacks in polar regions. *Nat Commun* **9,** 1919 (2018). https://doi.org/10.1038/s41467-018-04173-0

Graham, R.M. et al., 2017: Increasing frequency and duration of Arctic winter warming events. Geophysical Research Letters, **44** (13), 6974–6983, doi:10.1002/2017gl073395.

Groot Zwaaftink, C. D., H. Grythe, H. Skov, and A. Stohl (2016), Substantial contribution of northern high-latitude sources to mineral dust in the Arctic, J. Geophys. Res. Atmos., 121, 13,678–13,697, doi:10.1002/ 2016JD025482.

Hall, J. V., Loboda, T. V., Giglio, L., McCarty G. W. (2016), A MODIS-based burned area assessment for Russian croplands: Mapping requirements and challenges. Remote Sensing of Environment, Vol. 184, 506-521. https://doi.org/10.1016/j.rse.2016.07.022

Hansen J. and Nazarenko, L. (2004): Soot climate forcing via snow and ice albedos. PNAS, 101 (2). 423-428.

Hansen, E., Gerland, S., Granskog, M. A., Pavlova, O., Renner, A. H. H., Haapala, J., et al. (2013). Thinning of Arctic sea ice observed in Fram Strait: 1990–2011. Journal of Geophysical Research: Oceans, 118, 5202–5221. https://doi.org/10.1002/jgrc.20393

Herber, A., L. W. Thomason, H. Gernandt, U. Leiterer, D. Nagel, K. Schulz, J. Kaptur, T. Albrecht, and J. Notholt (2002), Continuous day and night aerosol optical depth observations in the Arctic between 1991 and 1999, J. Geophys. Res., 107(D10), 4097, doi:10.1029/2001JD000536.

Hesaraki S, O'Neill NT, Lesins G, Saha A, Martin RV, Fioletov VE, Baibakov K, Abboud I. Comparisons of a chemical transport model with a four-year (April to September) analysis of fine-and coarse-mode aerosol optical depth retrievals over the Canadian Arctic. Atmosphere-Ocean. 2017 Oct 20;55(4-5):213-29.

Hyer, E. J., J. S. Reid, and J. Zhang, 2011: An over-land aerosol optical depth data set for data assimilation by filtering, correction, and aggregation of MODIS Collection 5 optical depth retrievals. *Atmospheric Measurement Techniques*, European Geophysical Union, 379-408.

Hyer, Edward J., Eric S. Kasischke, and Dale J. Allen. "Effects of source temporal resolution on transport simulations of boreal fire emissions." *Journal of Geophysical Research: Atmospheres* 112.D1 (2007). https://doi.org/10.1029/2006JD007234

Hyer EJ, Reid JS, Prins EM, Hoffman JP, Schmidt CC, Miettinen JI, Giglio L. : Patterns of fire activity over Indonesia and Malaysia from polar and geostationary satellite observations *Atmospheric Research*. 122: 504-519.
DOI: 10.1016/J.Atmosres.2012.06.011 , 2013

Inness, A., Ades, M., Agustí-Panareda, A., Barré, J., Benedictow, A., Blechschmidt, A.-M., Dominguez, J. J., Engelen, R., Eskes, H., Flemming, J., Huijnen, V., Jones, L., Kipling, Z., Massart, S., Parrington, M., Peuch, V.-H., Razinger, M., Remy, S., Schulz, M., and Suttie, M.: The CAMS reanalysis of atmospheric composition, Atmos. Chem. Phys., 19, 3515–3556, https://doi.org/10.5194/acp-19-3515-2019, 2019.

IPCC 2013 Chapter 8 by Myhre, G., D. Shindell, F.-M. Bréon, W. Collins, J. Fuglestvedt, J. Huang, D. Koch, J.-F. Lamarque, D. Lee, B. Mendoza, T. Nakajima, A. Robock, G. Stephens, T. Takemura and H. Zhang, 2013: Anthropogenic and Natural Radiative Forcing. In: Climate Change 2013: The Physical Science Basis. Contribution of Working Group I to the Fifth Assessment Report of the Intergovernmental Panel on Climate Change [Stocker, T.F., D. Qin, G.-K. Plattner, M. Tignor, S.K. Allen, J. Boschung, A. Nauels, Y. Xia, V. Bex and P.M. Midgley (eds.)]. Cambridge University Press, Cambridge, United Kingdom and New York, NY, USA.

Iziomon, M. G., U. Lohmann, and P. K. Quinn (2006), Summertime pollution events in the Arctic and potential implications, J. Geophys. Res., 111, D12206, doi:10.1029/2005JD006223.

Jacob, D. J., J. H. Crawford, H. Maring, A. D. Clarke, J. E. Dibb, L. K. Emmons, R. A. Ferrare, C. A. Hostetler, P. B. Russell, and H. B. Singh (2010), The arctic research of the composition of the troposphere from aircraft and satellites (ARCTAS) mission: Design, execution, and first results, Atmos. Chem. Phys., 10(11), 5191–5212.

Jacobson, M. Z. (2004), Climate response of fossil fuel and biofuel soot, accounting for soot's feedback to snow and sea ice albedo and emissivity, J. Geophys. Res., 109, D21201, doi:10.1029/2004JD004945.

Kang S., Y. Zhang, Y. Qian, and H. Wang. 2020. "A review of black carbon in snow and ice and its impact on the cryosphere." *Earth - Science Reviews* 210. PNNL-SA-154137. doi:10.1016/j.earscirev.2020.103346

Kapsch, M.-L., R.G. Graversen and M. Tjernström, 2013: Springtime atmospheric energy transport and the control of Arctic summer sea-ice extent. Nature Climate Change, **3**, 744, doi:10.1038/nclimate1884.

Khan, A. L., S. Wagner, R. Jaffe, P. Xian, M. Williams, R. Armstrong, and D. McKnight (2017), Dissolved black carbon in the global cryosphere: Concentrations and chemical signatures, Geophys. Res. Lett., 44, 6226–6234, doi:10.1002/2017GL073485.

Kim, J. S., Kug, J. S., Jeong, S. J., Park, H., and Schaepman-Strub, G.: Extensive fires in southeastern Siberian permafrost linked to preceding Arctic Oscillation, Sci. Adv., 6, eaax3308, https://doi.org/10.1126/sciadv.aax3308, 2020.

Kim, M. H., and Coauthors, 2018: The CALIPSO version 4 automated aerosol classification and lidar ratio selection algorithm. *Atmospheric Measurement Techniques*, **11,** 6107-6135.

Kleidman, R. G., N. T. O'Neill, L. A. Remer, Y. J. Kaufman, T. F. Eck, D. Tanre´, O. Dubovik, and B. N. Holben (2005), Comparison of Moderate Resolution Imaging Spectroradiometer (MODIS) and Aerosol Robotic Network (AERONET) remote-sensing retrievals of aerosol fine mode fraction over ocean, J. Geophys. Res., 110, D22205, doi:10.1029/2005JD005760.

Kokhanovsky, A., and Tomasi, C. (Eds.): Physics and Chemistry of the Arctic Atmosphere. Springer Nature Switzerland AG 2020. https://doi.org/10.1007/978-3-030-33566-3

Köllner, F., Schneider, J., Willis, M. D., Schulz, H., Kunkel, D., Bozem, H., Hoor, P., Klimach, T., Helleis, F., Burkart, J., Leaitch, W. R., Aliabadi, A. A., Abbatt, J. P. D., Herber, A. B., and Borrmann, S.: Chemical composition and source attribution of sub-micrometre aerosol particles in the summertime Arctic lower troposphere, Atmos. Chem. Phys., 21, 6509–6539, https://doi.org/10.5194/acp-21-6509-2021, 2021.

Kondo, Y., et al. (2011), Emissions of black carbon, organic, and inorganic aerosols from biomass burning in North America and Asia in 2008, J. Geophys. Res., 116, D08204, doi:10.1029/2010JD015152.

Korontzi, S., J. McCarty, T. Loboda, S. Kumar, and C. Justice (2006), Global distribution of agricultural fires in croplands from 3 years of Moderate Resolution Imaging Spectroradiometer (MODIS) data, Global Biogeochem. Cycles, 20, GB2021, doi:10.1029/2005GB002529.

Kwok, R. and Rothrock D. A. (2009) Decline in Arctic sea ice thickness from submarine and ICESate records: 1958-2008. Geophys. Res. Lett. 36 L15501.

Law, K. S. and A. Stohl, 2007: Arctic air pollution: Origins and impacts. *Science*, **315**, 1537–1540, doi:10.1126/science.1137695.

Lubin, D., and Vogelmann, A. M. (2006). A climatologically significant aerosol longwave indirect effect in the Arctic. *Nature*, *439*, 453–456. https://doi.org/10.1038/nature04449

Lynch, P., J. S. Reid, D. L. Westphal, J. Zhang, T. Hogan, E. J. Hyer, C. A. Curtis, D. Hegg, Y. Shi, J. R. Campbell, J. Rubin, W. Sessions, J. Turk and A. Walker: An 11-year Global Gridded Aerosol Optical Thickness Reanalysis (v1.0) for Atmospheric and

Climate Sciences. Geosci. Model Dev., 9, 1489-1522, doi:10.5194/gmd-9-1489-2016, 2016.

Macias Fauria, M, E. A. Johnson, Large-scale climatic patterns control large lightning fire occurrence in Canada and Alaska forest regions. *J. Geophys. Res.* **111**, G04008 (2006).

Markowicz, K. M., et al. (2016), Impact of North American intense fires on aerosol optical properties measured over the European Arctic in July 2015, J. Geophys. Res. Atmos., 121, 14,487–14,512, doi:10.1002/2016JD025310.

Markowicz, K.M., Lisok, J., Xian, P., Simulation of long-term direct aerosol radiative forcing over the arctic within the framework of the iAREA project, Atmospheric Environment (2021), doi: https://doi.org/10.1016/j.atmosenv.2020.117882.

Mauritsen, T., Sedlar, J., Tjernström, M., Leck, C., Martin, M., Shupe, M., Sjogren, S., Sierau, B., Persson, P. O. G., Brooks, I. M., and Swietlicki, E.: An Arctic CCN-limited cloud-aerosol regime, Atmos. Chem. Phys., 11, 165–173, https://doi.org/10.5194/acp-11-165-2011, 2011.

McCarty, J. L., Aalto, J., Paunu, V.-V., Arnold, S. R., Eckhardt, S., Klimont, Z., Fain, J. J., Evangeliou, N., Venäläinen, A., Tchebakova, N. M., Parfenova, E. I., Kupiainen, K., Soja, A. J., Huang, L., and Wilson, S.: Reviews ~~& Syntheses~~and syntheses: Arctic ~~Fire Regimes~~fire regimes and ~~Emissions~~emissions in the 21st ~~Century~~century, Biogeosciences ~~Discuss. [preprint],~~, 18, 5053–5083, https://doi.org/10.5194/bg-18-5053-2021~~-83, in review~~, 2021.

McNaughton, C. S., Clarke, A. D., Freitag, S., Kapustin, V. N., Kondo, Y., Moteki, N., Sahu, L., Takegawa, N., Schwarz, J. P., Spackman, J. R., Watts, L., Diskin, G., Podolske, J., Holloway, J. S., Wisthaler, A., Mikoviny, T., de Gouw, J., Warneke, C., Jimenez, J., Cubison, M., Howell, S. G., Middlebrook, A., Bahreini, R., Anderson, B. E., Winstead, E., Thornhill, K. L., Lack, D., Cozic, J., and Brock, C. A.: Absorbing aerosol in the troposphere of the Western Arctic during the 2008 ARCTAS/ARCPAC airborne field campaigns, Atmos. Chem. Phys., 11, 7561–7582, https://doi.org/10.5194/acp-11-7561-2011, 2011.

Meier, W. N., Hovelsrud, G. K., van Oort, B. E. H., Key, J. R., Kovacs, K. M., Michel, C., et al. (2014). Arctic sea ice in transformation: A review of recent observed changes and impacts on biology and human activity. *Reviews of Geophysics*, **52**, 185– 217. https://doi.org/10.1002/2013RG000431

Morrison, A.L. et al., 2018: Isolating the Liquid Cloud Response to Recent Arctic Sea Ice Variability Using Spaceborne Lidar Observations. Journal of Geophysical Research: Atmospheres, **123** (1), 473–490, doi:10.1002/2017jd027248.

Notz D. and Stroeve, J. Observed Arctic sea-ice loss directly follows anthropogenic CO_2 emission (2016) *Science.* Vol. 354, Issue 6313, pp. 747-750 DOI: 10.1126/science.aag2345

Nummelin, A., C. Li and P.J. Hezel, 2017: Connecting ocean heat transport changes from the midlatitudes to the Arctic Ocean. Geophysical Research Letters, **44** (4), 1899–1908, doi:10.1002/2016GL071333.

O'Neill, N.T., T.F.Eck, B.N.Holben, A.Smirnov, O.Dubovik, and A.Royer (2001) Bimodal size distribution influences on the variation of Angstrom derivatives in spectral and optical depth space, J. Geophys. Res., 106, 9787-9806.

O'Neill, N. T., Perro, C., Saha, A., Lesins, G., Duck, T. J., Eloranta, E. W., Nott, G. J., Hoffman, A., Karumudi, M. L., Ritter, C., Bourassa, A., Abboud, I., Carn S., A., Savastiouk, V. (2012) Properties of Sarycheve Sulphate aerosols over the Arctic. J. Geophys. Res. Atmos. Vol. 117, D04203, https://doi.org/10.1029/2011JD016838

O'Neill, N. T., Eck, T. F., Smirnov, A., Holben, B. N., and Thulasiraman S. (2003) Spectral discrimination of coarse and fine mode optical depth. J. Geophys. Res., 108, D05212, doi:10.1029/2002JD002975.

Peterson, D. A., Fromm, M. D., Solbrig, J. E., Hyer, E. J., Surratt, M. L., & Campbell, J. R. (2017). Detection and Inventory of Intense Pyroconvection in Western North America using GOES-15 Daytime Infrared Data, Journal of Applied Meteorology and Climatology, 56(2), 471-493.

Peterson, D. A., Hyer, E. J., Campbell, J. R., Fromm, M. D., Hair, J. W., Butler, C. F., & Fenn, M. A. (2015). The 2013 Rim Fire: Implications for Predicting Extreme Fire Spread, Pyroconvection, and Smoke Emissions, Bulletin of the American Meteorological Society, 96(2), 229-247.

Perovich, D. K., and C. Polashenski (2012), Albedo evolution of seasonal Arctic sea ice, Geophys. Res. Lett., 39, L08501, doi:10.1029/2012GL051432

Prenni, A. J., Harrington, J. Y., Tjernström, M., DeMott, P. J., Avramov, A., Long, C. N., Kreidenweis, S. M., Olsson, P. Q., and Verlinde, J.: Can ice-nucleating aerosols affect arctic seasonal climate?, B. Am. Meteorol. Soc., 88, 541–550, https://doi.org/10.1175/BAMS-88-4-541, 2007.

Quinn, P. K., et al. (2008), Short-lived pollutants in the Arctic: Their climate impact and possible mitigation strategies, Atmos. Chem. Phys., 8(6), 1723–1735, doi:10.5194/acp-8-1723-2008.

Randles, C. A., daSilva, A. M., Buchard, V., Colarco, P. R., Darmenov, A., Govindaraju, R., et al.: The MERRA-2 aerosol reanalysis, 1980 onward. Part I: System description

and data assimilation evaluation. Journal of Climate, 30(17), 6823-6850. https://doi.org/10.1175/JCLI-D-16-0609.1, 2017.

Randerson, J. T., and Coauthors, 2006: The impact of boreal forest fire on climate warming. Science, 314, 1130–1132, doi:10.1126/science.1132075.

Ranjbar, K., O'Neill, N. T., Lutsch, E., McCullough, E. M., AboEl-Fetouh, Y., Xian, P., et al. (2019). Extreme smoke event over the high Arctic. *Atmospheric Environment*, *218*, 117002. https://doi.org/10.1016/j.atmosenv.2019.117002

Reid, J. S., Hyer, E. J., Prins, E. M., Westphal, D. L., Zhang, J., Wang, J., Christopher, S. A., Curtis, C. A., Schmidt, C. C., Eleuterio, D. P., Richardson, K. A., and Hoffman, J. P.: Global Monitoring and Forecasting of Biomass-Burning Smoke: Description of and Lessons from the Fire Locating and Modeling of Burning Emissions (FLAMBE) Program, IEEE J. Sel. Top. Appl., 2, 144–162, JSTARS-2009-00034, 2009.

Reid, J. S., Koppmann, R., Eck, T. F., and Eleuterio, D. P.: A review of biomass burning emissions part II: intensive physical properties of biomass burning particles, Atmos. Chem. Phys., 5, 799–825, https://doi.org/10.5194/acp-5-799-2005, 2005.

Rinke, A., Maturilli, M., Graham, R. M., Hatthes, H., Handorf, D., Cohen, L., Hudson, S. R. and Moore, J. C., (2017), Extreme cyclone events in the Arctic: Wintertime variability and trends. *Environ. Res. Lett.* **12** 094006

Rosel, A., Itkin, P., King, J., Divine, D., Wang, C., Granskog, M. A., Krumpen, T., and Gerland, S. (2018). Thin sea ice, thick snow and widespread negative freeboard observed during N-ICE2015 north of Svalbard. J. Geophys. Res: Oceans, 123, 1156–1176. https://doi.org/10.1002/2017JC012865

Saha, A., et al. (2010), Pan-Arctic sunphotometry during the ARCTAS-A campaign of April 2008, Geophys. Res. Lett., 37, L05803, doi:10.1029/2009GL041375.

Sand, M., T. K. Berntsen, Ø. Seland, and J. E. Kristjánsson (2013), Arctic surface temperature change to emissions of black carbon within Arctic or midlatitudes, J. Geophys. Res. Atmos., 118, 7788–7798, doi:10.1002/jgrd.50613.

Sand, M., Berntsen, T., Von Salzen, K., Flanner, M., Langner, J., and Victor, D.: Response of Arctic temperature to changes in emissions of short-lived climate forcers, Nat. Clim. Change, 6, 286–289, https://doi.org/10.1038/nclimate2880, 2016.

Sand, M., Samset, B. H., Balkanski, Y., Bauer, S., Bellouin, N., Berntsen, T. K., Bian, H., Chin, M., Diehl, T., Easter, R., Ghan, S. J., Iversen, T., Kirkevåg, A., Lamarque, J.-F., Lin, G., Liu, X., Luo, G., Myhre, G., Noije, T. V., Penner, J. E., Schulz, M., Seland, Ø., Skeie, R. B., Stier, P., Takemura, T., Tsigaridis, K., Yu, F., Zhang, K., and Zhang, H.: Aerosols at the poles: an AeroCom Phase II multi-model evaluation, Atmos. Chem. Phys., 17, 12197–12218, https://doi.org/10.5194/acp-17-12197-2017, 2017.

Sayer, A. M. and Knobelspiesse, K. D.: How should we aggregate data? Methods accounting for the numerical distributions, with an assessment of aerosol optical depth, Atmos. Chem. Phys., 19, 15023–15048, https://doi.org/10.5194/acp-19-15023-2019, 2019.

Serreze, M.C. and R.G. Barry, 2011: Processes and impacts of Arctic amplification: A research synthesis. Global and Planetary Change, **77** (1– 2), 85–96, doi:10.1016/j.gloplacha.2011.03.004.

Serreze, M.C., Francis, J.A. The Arctic Amplification Debate. *Climatic Change* **76,** 241–264 (2006). https://doi.org/10.1007/s10584-005-9017-y

Sharma, S., M. Ishizawa, D. Chan, D. Lavoué, E. Andrews, K. Eleftheriadis, and S. Maksyutov (2013), 16-year simulation of Arctic black carbon: Transport, source contribution, and sensitivity analysis on deposition, J. Geophys. Res. Atmos., 118, 943–964, doi:10.1029/2012JD017774.

Shi, Y., J. Zhang, J. S. Reid, E. J. Hyer, and N. C. Hsu, 2013: Critical evaluation of the MODIS Deep Blue aerosol optical depth product for data assimilation over North Africa. *Atmospheric Measurement Techniques*, **6,** 949-969.

Shi, Y., J. Zhang, J. S. Reid, B. Holben, E. J. Hyer, and C. Curtis, 2011: An analysis of the collection 5 MODIS over-ocean aerosol optical depth product for its implication in aerosol assimilation. *Atmos. Chem. Phys.*, **11,** 557-565.

Shindell, D. and Faluvegi, G.: Climate response to regional radiative forcing during the twentieth century, Nat. Geosci., 2, 294–300, https://doi.org/10.1038/ngeo473, 2009.

Schlosser, J. S., R. A. Braun, T. Bradley, H. Dadashazar, A. B. MacDonald, A. A. Aldhaif, M. A. Aghdam, A. H. Mardi, P. Xian, and A. Sorooshian (2017), Analysis of aerosol composition data for western United States wildfires between 2005 and 2015: Dust emissions, chloride depletion, and most enhanced aerosol constituents, J. Geophys. Res. Atmos., 122, 8951–8966, doi:10.1002/2017JD026547.

Skiles S. M., Flanner, M., Cook, J. M., Dumont, M. and Painter, T. (2018) Radiative forcing by light-absorbing particles in snow. Nature Climate Change, 8, 964-971. https://doi.org/10.1038/s41558-018-0296-5

Skinner, W. R., B. J. Stocks, D. L. Martell, B. Bonsal, and A. Shabbar, 1999: The association between circulation anomalies in the mid- troposphere and area burned by wildland fire in Canada. *Theoretical and Applied Climatology*, **63,** 89-105.

Stohl, A., et al. (2006), Pan-Arctic enhancements of light absorbing aerosol concentrations due to North American boreal forest fires during summer 2004, J. Geophys. Res., 111, D22214, doi:10.1029/2006JD007216.

Stohl, A., et al. (2007), Arctic smoke—Record high air pollution levels in the European Arctic due to agricultural fires in eastern Europe in spring 2006, Atmos. Chem. Phys., 7(2), 511–534, doi:10.5194/acp-7-511-2007.

Stone, R. S., G. P. Anderson, E. Andrews, E. G. Dutton, E. P. Shettle, and A. Berk (2007), Incursions and radiative impact of Asian dust in northern Alaska, Geophys. Res. Lett., 34, L14815, doi:10.1029/2007GL029878.

Taylor, P., B. Hegyi, R. Boeke and L. Boisvert, 2018: On the Increasing Importance of Air-Sea Exchanges in a Thawing Arctic: A Review. Atmosphere, **9** (2), doi:10.3390/atmos9020041.

Tomasi, C., Kokhanovsky, A. A., Lupi, A., Ritter, C., Smirnov, A., O'Neill, N. T., Stone, R. S., Holben, B. N., Nyeki, S., Wehrli, C., Stohl, A., Mazzola, M., Lanconelli, C., Vitale, V., Stebel, K., Aaltonen, V., de Leeuw, G., Rodriguez, E., Herber, A. B., Radionov, V. F., Zielinski, T., Petelski, T., Sakerin, S. M., Kabanov, D. M., Xue, Y., Mei, L., Istomina, L., Wagener, R., McArthur, B., Sobolewski, P. S., Kivi, R., Courcoux, Y., Larouche, P., Broccardo, S., & Piketh, S. J. (2015). Aerosol remote sensing in polar regions. *Earth-Science Reviews, 140*, 108–157. https://doi.org/10.1016/j.earscirev.2014.11.001.

Tomasi, C., Vitale, V., Lupi, A., Di Carmine, C., Campanelli, M., Herber, A., Treffeisen, R., Stone, R. S., Andrews, E., Sharma, S., Radionov, V., von Hoyningen-Huene, W., Stebel, K., Hansen, G. H., Myhre, C. L.,Wehrli, C., Aaltonen, V., Lihavainen, H., Virkkula, A., Hillamo, R., Ström, J., Toledano, C., Cachorro, V. E., Ortiz, P., de Frutos, A. M., Blindheim, S., Frioud, M., Gausa, M., Zielinski, T., Petelski, T., & Yamanouchi, T. (2007). Aerosols in polar regions: a historical overview based on optical depth and in situ observations. *Journal of Geophysical Research, Atmospheres, 112*, D16. https://doi.org/10.1029/2007JD008432.

Thomason, L. W., Ernest, N., Luis, M. L., Rieger, L., Bourassa, A., Vernier, J.-P., Manney, G., Luo, B., Arfeuille, F., & Peter, T. (2018). A global space-based stratospheric aerosol climatology: 1979–2016. *Earth System Science Data, 10*, 469–492. https://doi.org/10.5194/essd-10-469-2018.

Torres, O., Bhartia, P. K., Taha, G., Jethva, H., Das, S., Colarco, P., Krotkov, N., Omar, A., and Ahn, C.: Stratospheric Injection of Massive Smoke Plume From Canadian Boreal Fires in 2017 as Seen by DSCOVR-EPIC, CALIOP, and OMPS-LP Observations, J. Geophys. Res.-Atmos., 125, e2020JD032579, https://doi.org/10.1029/2020JD032579, 2020.

Toth, T. D., Campbell, J. R., Reid, J. S., Tackett, J. L., Vaughan, M. A., Zhang, J., & Marquis, J. W. (2018). Minimum aerosol layer detection sensitivities and their subsequent impacts on aerosol optical thickness retrievals in CALIPSO level 2 data products. *Atmospheric Measurement Techniques*, *11*(1), 499-514.

Toth, T. D., Zhang, J., Campbell, J. R., Reid, J. S., & Vaughan, M. A. (2016). Temporal variability of aerosol optical thickness vertical distribution observed from CALIOP. *Journal of Geophysical Research: Atmospheres*, *121*(15), 9117-9139.

Valkonen, E., Cassano, J., & Cassano, E. (2021). Arctic cyclones and their interactions with the declining sea ice: A recent climatology. Journal of Geophysical Research: Atmospheres, 126, e2020JD034366. https://doi.org/10.1029/2020JD034366

van der Werf, G. R., J. T. Randerson, L. Giglio, G. J. Collatz, P. S. Kasibhatla, and A. F. Arellano Jr., 2006: Interannual variability in global biomass burning emissions from 1997 to 2004. Atmos. Chem. Phys., 6, 3423–3441, doi:10.5194/acp-6-3423-2006.

Warneke, C., Froyd, K. D., Brioude, J., Bahreini, R., Brock, C. A., Cozic, J., et al. (2010). An important contribution to springtime Arctic aerosol from biomass burning in Russia. *Geophysical Research Letters*, *37*, L01801. https://doi.org/10.1029/2009GL041816

Waseda, T., Nose, T., Kodaira, T, Sasmal, K and Webb, A. (2021) Climatic trends of extreme wave events caused by Arctic cyclones in the western Arctic Ocean. Polar Science. Vol 27, 100625, doi:10.1016/j.polar.2020.100625

Wendisch, M., Macke, A., Ehrlich, A., Lupkes, C., Mech, M., Chechin, D., et al. (2019). The Arctic cloud puzzle: Using ACLOUD/PASCAL multiplatform observations to unravel the role of clouds and aerosol particles in Arctic amplification. *Bulletin of the American Meteorological Society*, *100*, 841–871. https://doi.org/10.1175/BAMS-D-18-0072.1

Wex, H., Huang, L., Zhang, W., Hung, H., Traversi, R., Becagli, S., Sheesley, R. J., Moffett, C. E., Barrett, T. E., Bossi, R., Skov, H., Hünerbein, A., Lubitz, J., Löffler, M., Linke, O., Hartmann, M., Herenz, P., and Stratmann, F.: Annual variability of ice-nucleating particle concentrations at different Arctic locations, Atmos. Chem. Phys., 19, 5293–5311, https://doi.org/10.5194/acp-19-5293-2019, 2019.

Winker, D. M., Pelon, J. R., & McCormick, M. P. (2003, March). CALIPSO mission: spaceborne lidar for observation of aerosols and clouds. In *Lidar Remote Sensing for Industry and Environment Monitoring III* (Vol. 4893, pp. 1-11). International Society for Optics and Photonics.

Woods, C., & Caballero, R. (2016). The role of moist intrusions in Winter Arctic warming and sea ice decline. *Journal of Climate*, *29*, 4473–4485. https://doi.org/10.1175/JCLI-D-15-0773.1

Xian, P., Klotzbach, P. J., Dunion, J. P., Janiga, M. A., Reid, J. S., Colarco, P. R., and Kipling, Z.: Revisiting the relationship between Atlantic dust and tropical cyclone activity using aerosol optical depth reanalyses: 2003–2018, Atmos. Chem. Phys., 20, 15357–15378, https://doi.org/10.5194/acp-20-15357-2020, 2020.

Xian, P., Reid J. S., Hyer, E., Sampson, C.R., Rubin,J., Ades M., et. al., Current state of the global operational aerosol multi-model ensemble: an update from the International Cooperative for Aerosol Prediction (ICAP), 2019, Quarterly J. of the Royal Met. Soc. https://doi.org/10.1002/qj.3497

Xian, P., J. S. Reid, J. F. Turk, E. J. Hyer and D. L. Westphal: Impact of models versus satellite measured tropical precipitation on regional smoke optical thickness in an aerosol transport model, *Geophys. Res. Lett.*, 36, L16805, doi:10.1029/2009GL038823, 2009.

Yang, Y., Wang, H., Smith, S. J., Easter, R. C., and Rasch, P. J.: Sulfate Aerosol in the Arctic: Source Attribution and Radiative Forcing, J. Geophys. Res.-Atmos., 123, 1899–1918, https://doi.org/10.1002/2017JD027298, 2018.

Zamora, L. M., Kahn, R. A., Cubison, M. J., Diskin, G. S., Jimenez, J. L., Kondo, Y., McFarquhar, G. M., Nenes, A., Thornhill, K. L., Wisthaler, A., Zelenyuk, A., and Ziemba, L. D.: Aircraftmeasured indirect cloud effects from biomass burning smoke in the Arctic and subarctic, Atmos. Chem. Phys., 16, 715–738, https://doi.org/10.5194/acp-16-715-2016, 2016.

Zhang, J. L., and J. S. Reid, 2006: MODIS aerosol product analysis for data assimilation: Assessment of over-ocean level 2 aerosol optical thickness retrievals. *J. Geophys. Res.-Atmos.*, **111**.

Zhang, J. L., and J. S. Reid, D. L. Westphal, N. L. Baker, and E. J. Hyer, 2008: A system for operational aerosol optical depth data assimilation over global oceans. J. Geophys. Res., 113, D10208, doi:10.1029/2007JD009065.

Zhang, J. and Reid, J. S.: A decadal regional and global trend analysis of the aerosol optical depth using a data-assimilation grade over-water MODIS and Level 2 MISR aerosol products, Atmos. Chem. Phys., 10, 18879-18917, doi:10.5194/acpd-10-18879-2010, 2010.

Zhang J., Reid, J. S., Alfaro-Contreras, R., Xian P., Has China been exporting less particulate air pollution over the past decade?, *Geophysical Research Letters*, 10.1002/2017GL072617, 2017.

Zhang, J., Spurr, R. J. D., Reid, J. S., Xian, P., Colarco, P. R., Campbell, J. R., Hyer, E. J., and Baker, N. L.: Development of an Ozone Monitoring Instrument (OMI) aerosol index (AI) data assimilation scheme for aerosol modeling over bright surfaces – a step toward direct radiance assimilation in the UV spectrum, Geosci. Model Dev., 14, 27–42, https://doi.org/10.5194/gmd-14-27-2021, 2021.

Zhao, C., & Garrett, T. J. (2015). Effects of Arctic haze on surface cloud radiative forcing. *Geophysical Research Letters*, *42*, 557–564. https://doi.org/10.1002/2014GL062015

Zhang, Z.; Wang, L.; Xue, N.; Du, Z. Spatiotemporal Analysis of Active Fires in the Arctic Region during 2001–2019 and a Fire Risk Assessment Model. *Fire* **2021**, *4*, 57. https://doi.org/10.3390/fire4030057